Chapter 2
High-Order Harmonic Generation from Laser Ablation of Various Surfaces

The high-order harmonic generation in laser-produced plasma plumes can be useful for producing an efficient source of short-wavelength ultra-short pulses for various applications and studies of the properties of harmonic emitters. The laser ablation induced high-order harmonic generation spectroscopy is a new method for the studies of material science. We discuss the realization of new ideas, which further improved the frequency conversion efficiency through harmonic generation in specially prepared plasmas and allowed the spectral and structural studies of matter through the plasma harmonic spectroscopy. We also present the current status of plasma harmonic studies, and show new trends in the developments of this filed. In particular, we show new approaches in high-order harmonic generation from various plasmas for the studies of the physical properties of materials.

Coherent short wavelength radiation is of increasing importance for a broad variety of basic and applied research in various fields of physical, chemical, and life sciences. Among them, femtosecond time-resolved coherent diffractive imaging and photo-induced processes at surfaces and nanoparticles, as well as lithography, plasma diagnostics, and materials science processing and diagnostics are of foremost interest. The process of high-order harmonic generation from femtosecond visible laser pulses allows producing coherent radiation in the extreme ultraviolet spectral range. Table-top lasers render these processes possible with the prospect of wide-spread scientific applications. Presently predominantly few gases are employed as target media for HHG. Other efforts rely on the creation of harmonics at solid surfaces at relativistic laser intensities above $10^{18-19}\,\mathrm{W\,cm^{-2}}$ and with extremely high pulse contrast ratio, either by a coherent wake field excitation or, for petawatt class lasers, on a relativistically moving electron gas acting as a plasma mirror. So far, however, only low conversion efficiencies have been obtained, despite the enormous efforts. Other methods include XUV free-electron lasers (FELs) and X-ray lasers.

To promote the use of XUV radiation it seems therefore appropriate to advance laboratory scale sources to a higher application level. Many interesting experiments can be performed by HHG based on laboratory scale femtosecond lasers. These sources easily cover the spectral range between 10 and 100 eV photon energy of harmonics, and with few-cycles laser systems even up to several 100 eV. For practical

R. A. Ganeev, *Nonlinear Optical Properties of Materials*,
Springer Series in Optical Sciences 174, DOI: 10.1007/978-94-007-6022-6_2,

applications of high-order harmonic sources a higher conversion efficiency and thus an increase in the photon flux and also of the maximum photon energy of the harmonic radiation would be beneficial. HHG itself can be used as a spectroscopic tool for analysis of optical, nonlinear optical and structural properties of the emitters of harmonic generation presently comprising on a few noble gases. The generation of high harmonics in laser-produced plasmas on various solid-state targets, being for this purpose a relatively new and largely unexplored medium, promises to yield these advances.

Plasma HHG can open new doors in many unexpected areas of light-matter interaction. Besides considering as an alternative method for generation of coherent XUV radiation, it can be used as a powerful tool for various spectroscopic and analytical applications. A few of them have already emerged during recent years of plasma HHG studies. The application of doubly charged ions for high-order harmonic generation showed a promising extension of the cut-off photon energy in plasma harmonics, without having to rely on few-cycle driving pulses. As it has been shown in the case of low-order harmonics, the conversion efficiency can be strongly enhanced by making use of resonances in atomic or ionic systems. This has been demonstrated in pioneering plasma harmonic experiments using the indium and other metals. For laser-generated plasmas a large variety of materials can be employed, thereby increasing the chance to select such resonances with fixed-frequency Ti:sapphire lasers. Furthermore, it has been shown that two-colour pumping profitably enhances the high-harmonic intensity and significantly influences the output and properties of harmonic spectrum in rare gases. For plasma harmonics, where this technique has recently been adopted, this will be a new approach for the nonlinear spectroscopy of ionic transitions possessing high oscillator strengths.

Most interestingly, recent studies have shown that enhanced high-order harmonics can be generated also from the ablated nanoparticles, which opens the prospects for applications of local field enhancement, broad plasmonic resonances and a more efficient recombination processes for plasma HHG. As a highly interesting perspective an increase of the harmonic output by quasi phase matching in specially prepared plasmas may be considered. For the plasma a different and more flexible technique than used in neutral gases can be applied. The plasma may be spatially modified using a long pulse co-propagating with the fundamental driving pulse, and conditions might be found where quasi phase matching is possible over a long distance in the plasma, while the constructive and destructive interference in such plasmas containing different emitters can provide a new knowledge about the phase-related characteristics of this process.

Thus the above approach can be useful for producing an efficient source of short-wavelength ultra-short pulses for various applications and studies of the properties of harmonic emitters. The laser ablation induced high-order harmonic generation spectroscopy is a new method for the studies of material science and one of the most important applications of HHG. In this chapter, we discuss the realization of new ideas, which further improved the HHG efficiency through harmonic generation in specially prepared plasmas and allowed the spectral and structural studies of matter through the plasma harmonic spectroscopy. We also present the current status of

plasma HHG studies, and show new trends in the developments of this filed. In particular, we show new approaches in HHG from various plasmas for the studies of physical properties of materials.

2.1 Current Status of Plasma Harmonic Studies

High-order harmonic generation may presently be considered the simplest and most efficient technique of obtaining coherent short-wavelength radiation in a broad spectral range [1–9]. As it was already mentioned, alternative means in this area are the use of X-ray lasers [10, 11] and FELs [12]. However, unlike sources involving harmonic generation, X-ray lasers have been unable to generate radiation in a broad range of the extreme ultraviolet spectral domain. Other disadvantages of X-ray lasers are their poor spatial coherence and radiation divergence. As regards FELs that generate radiation in the XUV spectral range, there are only a few such lasers, which are limited in number. Furthermore, the application of these lasers is largely restricted by their extremely high development and maintenance cost.

HHG research is actively being pursued due to the availability of new high-power compact laser systems offering high output parameters (high energy and intensity of pulses and a high pulse repetition rate). Two mechanisms are used for HHG: harmonic generation in gases [1, 3–7] and from surfaces [2, 8, 9]. The considerable progress achieved in this area has enabled extending the range of generated coherent radiation toward the spectral region where the radiation can pass through water-bearing components (the so-called water window, 2.3–4.6 nm [6, 7]). This circumstance is attractive from the standpoint of the practical use of coherent short-wavelength radiation in studies of biological objects. However, the data on the generation of such radiation obtained to date with the use of the above techniques have exhibited a low conversion efficiency to the XUV range (10^{-6} and below), which considerably limits their practical use. This is supposedly the reason why in the last few years the emphasis has been placed on the optimisation of another effect discovered in these investigations, the generation of attosecond pulses [13].

The search for ways of increasing the HHG efficiency in the XUV spectral range has long been (and still is) among the most topical problems of nonlinear optics. However, in the majority of cases, the efficiency of conversion to high-order harmonics turns out to be insufficient for using them as real coherent short-wavelength radiation sources in biology, plasma diagnostics, medicine, microscopy, photolithography, XUV coherent diffraction imaging, time-resolved measurements, etc. The feasibility of increasing the intensities of high-order harmonics generated in gas jet sources by using atomic and ion resonances has been studied primarily by theoretical methods [14, 15]. The results of a number of calculations suggest that the intensity of harmonic may be substantially increased when this harmonic is at resonance with transitions in the atomic and ion spectra of gases. This approach, which yet been realized in the gas HHG, may be an alternative (or a complement) to the method of wave phase matching for harmonics and laser radiation [6, 7].

The first experiments on HHG in the passage of laser radiation through the plasma produced at the surface of a solid target carried out during first half of nineties turned out to be much less successful. As noted in a review on the bifurcational properties of harmonics in plasmas, "the effect of harmonic generation (in plasmas) calls for a more careful consideration and an in-depth basic research" [16]. Data obtained with the use of highly excited plasmas containing multiply charged ions revealed several limiting factors, which did not permit generating harmonics of a sufficiently high order and strong intensity [17–22]. Moreover, the harmonic intensity distribution did not correspond to the so-called three-step model of HHG [23], according to which a plateau-like high-order harmonic intensity distribution (i.e., of approximately equal intensity) should be observed. Those studies, which were carried out in the mid-1990s, stopped at the demonstration of relatively low-order harmonics (from the 11th through the 25th). This disadvantage, as well as the low conversion efficiency, led to the erosion of interest in this HHG technique, especially in comparison with the achievements involving gas sources of HHG.

Nevertheless, there is a reason to hope that harmonic intensities may be increased and efficient shorter-wavelength coherent radiation may be obtained using laser-produced plasmas. There are no fundamental limitations here; it only remains to find the optimal conditions for producing a plasma plume to serve as the efficient nonlinear medium for HHG. Laser-produced plasma may be validly used for this process if the effect of the limiting factors (self-defocusing, self phase modulation, and wave phase mismatch of the harmonics and the radiation being converted) is minimized [17, 21, 22].

Among the special features of HHG in laser-produced plasmas, we first of all note a wide range of nonlinear medium characteristics available by varying the conditions of laser plume production on the surface of a solid. This applies to plasma parameters such as the plasma dimension, the density of ions, electrons, and neutral particles, and the degree of their excitation. The use of any elements of the periodic table that exist as solids largely extends the range of materials employed, together with thousands of complex solid-state samples, whereas only a few light rare gases are typically used in gas HHG. Thus the exploration of practically any available solid-state material through the nonlinear spectroscopy comprising laser ablation and harmonic generation can be considered as a new tool for materials science.

In several cases, this method furnishes an opportunity to realize quasi-resonance conditions for increase in the efficiency of single harmonic generation due to the effect of ion transitions on the nonlinear response in the spectral range in question, thus allowing the studies of ionic transitions possessing strong oscillator strengths. This effect can hardly be observed in gas HHG because of a low probability for the coincidence of the atomic transition frequencies of few gases and the frequencies of single harmonics. The advantages of plasma HHG could largely be realized with the use of a low-excited and weakly ionised plasma, because the limiting processes governing the dynamics of laser wavelength conversion would play a minor role in this case. This assumption has been confirmed by several studies concerned with high-order harmonic generation in the plasma media [24–28]. A substantial increase in the highest order of the generated harmonics, the observation of long plateau and

emergence of a second plateau in the energy distribution of highest-order harmonics, the high efficiencies obtained with several plasma formations, the realization of resonance enhancement of individual harmonics, the efficient harmonic enhancement from plasma plumes containing clusters of different materials, and other properties revealed in those and other works [29–32] have demonstrated the advantages of using specially prepared plasmas for HHG. The orders of harmonics obtained in plasma media to date range into the sixties and seventies [24, 26, 33, 34]. The highest-order harmonics (the 101st order, wavelength 7.9 nm) have been demonstrated in manganese plasmas [35]. The HHG conversion efficiency in the plateau region amounted to 10^{-5} [36]. In addition to that, the efficiency of conversion to an individual (resonantly enhanced) high-order harmonic approached 10^{-4} [25, 26].

The quest for new plasma media that would favour the enhancement of an individual harmonic allows further enhancement of harmonic conversion efficiency. The production of a single high-intensity harmonic (rather than a group of harmonics of equal intensity in the plateau region) would open up the way to the practical application of these coherent short-wavelength radiation sources. Resonantly enhanced harmonics observed in several plasma media allowed expecting that similar conditions will be discovered for other plasma formations. The generated harmonic wavelength may then be tuned to the transitions with high oscillator strength by wavelength tuning of the driving laser [25, 31], as well as by varying the chirp of the laser radiation [26, 28, 30]. Application of ablated nanoparticles and clusters for HHG can also enhance the yield of harmonics in the XUV range. Further improvements in HHG conversion efficiency and harmonic extension require a systematic study of the influence of various plasma and laser parameters on ablation harmonics. Many new peculiarities of plasma harmonics emerged during last few years [37–73] allow expecting further extension of our knowledge of materials properties using this powerful took of nonlinear spectroscopy.

The future developments in the application of this technique may include such areas as the seeding of plasma resonance harmonics in the XUV free electron lasers, plasma-induced harmonic generation using a few-cycle pulses, application of endohedral fullerenes for plasma HHG, comparative studies of gas- and plasma-induced harmonics, analysis of molecular structures through the study of harmonic spectra from oriented molecules in plasmas, search for quasi-phase matching schemes in plasma plumes, use of single harmonic for the surface science, structural analysis of the multi-dimensional formations in laser plasma, generation of strong combs and single attosecond pulses, quest for quasi-solid-state HHG, application of the double-target schemes for plasma formation, use of rotating targets for improvements of harmonic stability, application of IR (1–3 μm) laser sources for extension of plasma harmonic cutoffs, analysis of plasma components through the HHG, etc.

The reviews on plasma harmonics studies were mostly devoted to the discussion of such specific topics as the application of the nanoparticle-containing plasmas for the HHG [41], resonance-induced enhancement of harmonics [74] and applications of fullerenes as the attractive media for harmonic generation [51], contrary to the two first topical reviews [42, 75], where the whole range of plasma harmonics studies was presented. It seems timely to return back to the practice of showing the broad

pattern of various developments in this field [67, 69, 76]. It is also obvious that the comprehensive overview of most recent findings can help in defining the next steps of the development in this relatively new and attractive area of nonlinear optical studies.

Whilst the first stage of these successful studies was entirely focused on the improvements of harmonic yield from plasma, at current stage of knowledge of the high-order nonlinear optical processes in ablation plume one can consider this method as a new tool for material science. Thus the search of the dual role of plasma HHG as a method for efficient coherent XUV light generation and of materials probing is a milestone of further developments in this field. Below, we show new trends emerged during recent years, which demonstrate the attractiveness of this method.

2.2 Harmonic Generation of Picosecond Nd:YAG Laser Radiation in Ablation-Produced Plasmas

As it was already pointed out, the advantages of HHG of laser radiation in a plasma plume could largely be realized with the use of low-excited and weakly ionized plasma, because in that case the limiting processes governing the dynamics of the laser frequency conversion would play a minor role [75]. A search for the best experimental conditions, such as pulse duration of driving laser field, for efficient HHG in different spectral ranges is a way for further enhancement of harmonic yield.

Previous plasma HHG studies were carried out using femtosecond pulses. The spectral range of those experiments was restricted at the longer wavelength side to ~80 nm, which was defined by the registration properties of the commonly used detectors of harmonic spectra (microchannel plates). A limited number of studies of plasma HHG had been performed in the spectral region above this wavelength. A search for resonance enhancement of single harmonic in these conditions can be justified by the presence of strong ionic and neutral transitions in the longer wavelength vacuum ultraviolet range (80–200 nm). Next, the application of longer pulses could avoid the impeding processes restricting the efficiency of harmonic generation in this region. There two main limiting processes, which can decrease the conversion efficiency in the ionic medium. The first one is an excess free electron concentration caused by over-excitation of the target surface. The appearance of a considerable number of free electrons is a result of ionization of both neutral atoms and singly charged particles. This follows with self-defocusing of the propagating probe pulse. The second process is directly related with the first one. The phase matching conditions of the driving and harmonic waves, which are maintained for a moderate number of free electrons appearing during ionization of neutrals, break up due to the increase of free electron concentration. This increase occurs abruptly once the fluence of the heating pulse reaches the threshold level, when the over-excitation of targets leads to the appearance of doubly and higher charged particles. Further, the use of longer pulses can also increase the fluence of harmonic emission at comparable

HHG conversion efficiencies from picosecond and femtosecond sources due to the higher pulse energies available in the former case.

Recent studies have shown the attractiveness of application of the long laser pulses for third-order harmonic generation from laser plasmas [68, 77]. Below we present an analysis of the HHG in various plasmas using 1064 nm, 38 ps pulses [78]. The goal of those studies was a search for the conditions for generation of energetic coherent picosecond pulses in the range of 80–220 nm using various metal-containing plasma plumes.

A passive mode-locked Nd:YAG laser (1064 nm, 1.5 Hz pulse repetition rate) generated a 38 ps pulse. Two-stage amplification of the single pulse was followed by splitting of this radiation into two parts, one (heating pulse) with an energy of 5 mJ, which was used for plasma formation on the target surface, and another (probe pulse) with an energy of up to 28 mJ, which was used after some delay for frequency conversion in various plasma plumes (Fig. 2.1). The heating pulse was focused using a 300 mm focal length lens inside the vacuum chamber containing various targets. The plasma sizes were in the range of 0.5 mm. The heating pulse intensity on the target surface was in the range of 10^{11} W cm^{-2}. The diameter of the single mode probe beam was 4 mm. This beam was focused inside the plasma plume using a 150 mm focal length lens. The probe beam propagated at a distance of 100–150 μm from the surface of the target. The intensity of the probe pulse at the focus was 4×10^{13} W cm^{-2}. The focal spot was inside the plasma plume. The delay between the heating and probe pulses during most of the experiments was maintained at 25 ns, which was optimal for efficient harmonic generation in metal-containing plasmas. The harmonic radiation was analyzed using a vacuum monochromator.

Various metal materials (copper, chromium, zinc, niobium, silver, indium, molybdenum, titanium, tin, lead, tantalum, manganese, tungsten, gold, boron and aluminum) were used as the targets for laser-induced plasma formation. A three-coordinate translating stage allowed movement of the target along the z-axis and control of the interaction zone of the probe radiation with the plasma relative to the target plane.

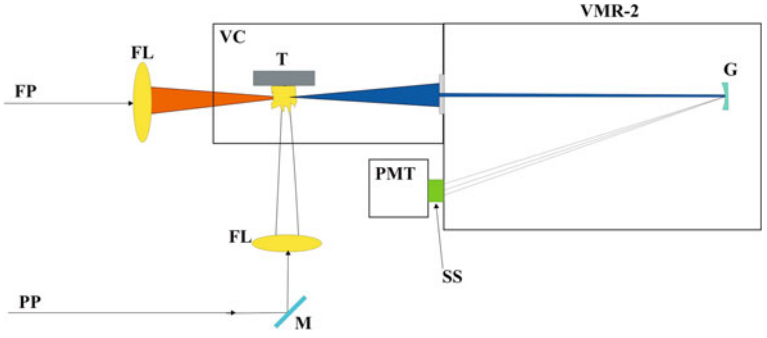

Fig. 2.1 The experimental setup for HHG in a laser plasma using picosecond pulses. *FP*, fundamental probe picosecond pulse; *PP*, heating picosecond pulse; *M*, mirror; *FL*, focusing lenses; *VC*, vacuum chamber; *T*, target; *VMR-2*, vacuum monochromator; *G*, grating; *SS*, sodium salicylate; *PMT*, photomultiplier tube. Reproduced from [78] with permission from IOP Publishing

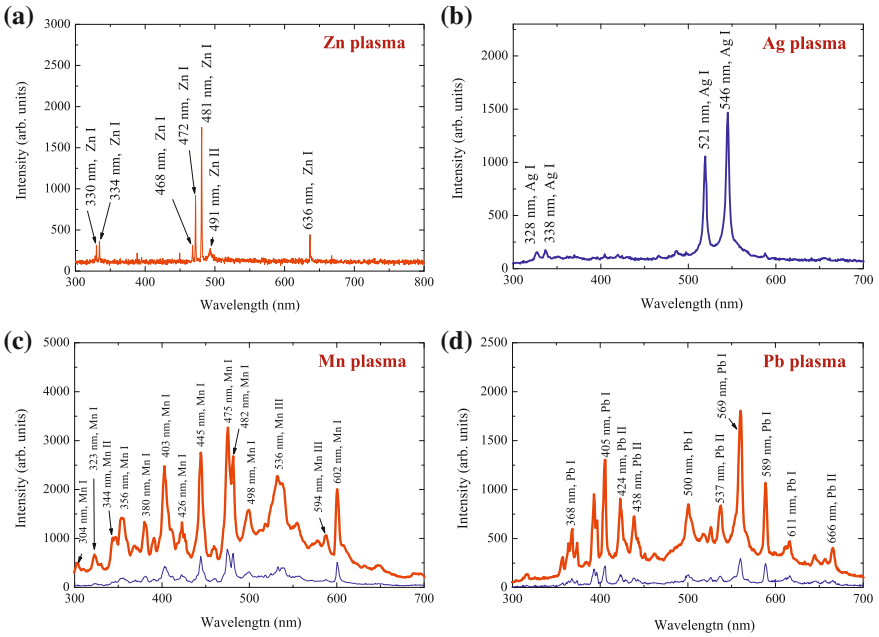

Fig. 2.2 Emission spectra from the (**a**) Zn and (**b**) Ag plasmas used for harmonic generation and plasma emission spectra from the (**c**) Mn and (**d**) Pb targets at weak (*thin lines*, $I = 8\times10^{10}$ W cm^{-2}) and strong (*thick lines*, $I = 2 \times 10^{11}$ W cm^{-2}) excitation of target surfaces. Adopted from [78] with permission from IOP Publishing

Analysis of the evolution of the spectra for the diagnosing laser plasma provides important information about the plasma parameters and can be used for multiple applications. In particular, some time-resolved laser-induced plasma spectrometry studies during harmonic studies from gold, silver, manganese and vanadium plasmas [37] allowed for identification of the emissions from native species and optimization of conditions when the plasma mostly consisted of excited neutrals and singly charged ions. It may be noted that most plasma HHG studies were carried out using time-integrated methods of plasma emission analysis, so it was impossible to define exactly what plasma conditions existed during the propagation of the femtosecond pulse through the plume. Below, we discuss a time-integrated analysis of spectral studies of plasma emission from various metal targets used for harmonic generation during propagation of the picosecond radiation through the plasma. These studies were aimed at defining the optimal plasma conditions for efficient HHG in laser plumes and showed that, while, for most plasma plumes, over-excitation during laser ablation leads to drastic decrease of harmonic generation efficiency, in some cases one can achieve the conditions for extension of the harmonic cutoff using picosecond probe pulses.

The spectral studies of atomic and ionic emission from the laser-produced plasmas were carried out in the visible and near ultraviolet ranges (300–700 nm). This spectral region was chosen due to the existence of multiple ionic and atomic transitions of

the studied plasma species. To create the ablation, a 1064 nm, 38 ps pulse from a Nd:YAG laser was focused onto a metal target in the vacuum chamber. The spectral characteristics of the laser plasma in the visible and UV ranges were analyzed using a fiber spectrometer (HR4000).

The spectra of plasma emission from the Zn and Ag plasmas are presented in Fig. 2.2a. One can note that these spectra were obtained at the conditions of 'optimal plasma' formation from the point of view of best HHG conversion efficiency. In this way, the maximum yield of harmonics was obtained, especially in the 80–220 nm range, and then the spectral characteristics of the laser plasmas were measured at these conditions. The spectral lines were mostly originated from the excited states of neutral and singly charged ions, when the impeding influence of free electrons on the high-order nonlinear optical processes in the laser plasmas was insignificant.

The increase of heating pulse intensity on the target surfaces above 10^{11} W cm^{-2} led to both the growth of emission intensity for neutral and singly charged ionic species and the appearance of emission lines from the higher charged particles. The appearance of doubly and triply charged ions and a large number of free electrons immediately followed with a considerable decrease of HHG conversion efficiency from almost all the plasma samples. The variations of the plasma spectra in that case are presented in Fig. 2.2b, where one can see the changes of intensity of plasma emission from the Pb and Mn targets. The thin and thick curves correspond to weak and strong excitation, correspondingly. This figure clearly shows the increase of the intensities of the Mn III and Pb II lines, which is correlated with an increase of the concentration of multiply charged ions in the plasma plume and correspondingly the concentration of free electrons.

Previous studies of HHG from plasma plumes have analyzed the UV emission spectra from the plasma to prove that over-excited and over-ionized plasmas could dramatically decrease the harmonic intensity [75]. However, as was mentioned above, these spectral measurements were performed using time-integrated methods that did not allow identification of the plasma state before the interaction with the delayed femtosecond pulse. One can note that the application of time-resolved laser-induced plasma spectrometry allowed previously the definition of the plasma conditions for the extension of harmonic cut-offs [37]. The application of this time-resolved technique, which was not available in the discussed studies [78], could further define better conditions of plasma HHG.

In [78], the restricting features of harmonic generation dynamics during over-excitation of the targets were observed in the case of most of the analyzed plasma plumes. The increase of heating pulse intensity from 1×10^{11} to 3×10^{11} W cm^{-2} during HHG experiments with these targets led to the appearance of strong plasma emission. At these excitation conditions, the harmonic emission from various plasmas was overlapped with the plasma emission. The intensity of the generated harmonics became considerably less than at 1×10^{11} W cm^{-2} excitation. In the case of most of the plasmas, this over-excitation led to a complete disappearance of harmonic emission. The variations of HHG efficiency with the growth of heating pulse intensity are depicted in Fig. 2.3. In particular, the 11th harmonic generated from the Pb plasma started to decrease with growth of the heating pulse energy above 3 mJ (Fig. 2.3a),

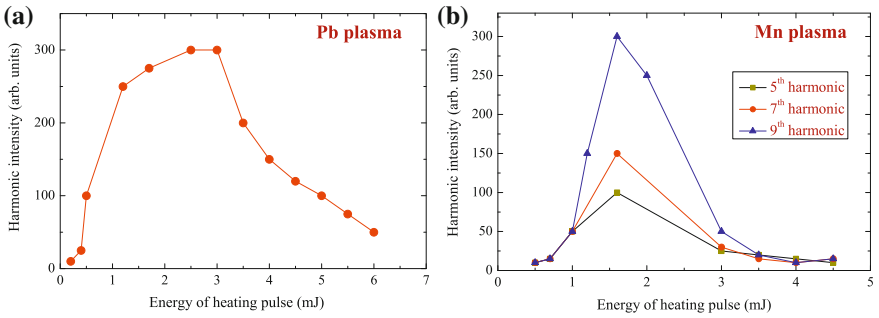

Fig. 2.3 Dependences of harmonic intensity at different heating pulse energies for the (**a**) 11th harmonic generating from the Pb plasma, and (**b**) 5, 7, and 9th harmonics generating from the Mn plasma. Reproduced from [78] with permission from IOP Publishing

which corresponds to an intensity of 1×10^{11} W cm^{-2}. In another case, a decrease of the 5, 7 and 9th harmonics generated in Mn plasma was observed at pulse energies above 1.5 mJ (Fig. 2.3b).

The reason for the decrease of harmonic conversion efficiency is related to over-excitation of the target, which leads to the appearance of an abundance of free electrons in the plasma plume. The latter cause a phase mismatch between the waves of the driving field and the harmonics. This effect is especially important for the lower-order harmonics. One can note that a decrease of harmonic efficiency with over-excitation of plasma has been reported for higher-order harmonics as well [75], although this decrease of converted XUV radiation was less abrupt than that observed in the present studies.

The characteristic pattern of almost all the harmonic spectra from metal plasmas was a featureless sharp decrease of conversion efficiency for lowest orders, which followed with a gradual decrease of higher harmonics (above the 9th order) up to the limit of the registration range of monochromator (50 nm, 21st harmonic). Figure 2.4 shows the characteristic HHG spectra obtained from Cr, Cu and Ti plasmas. Most of these plasmas showed comparable nonlinear optical properties from the point of view of HHG conversion efficiency.

Measurements of the absolute values of the conversion efficiencies of the harmonics generated in the plasmas were carried out using the following procedure. In the first step, the 4th harmonic signal was measured by a 'monochromator + sodium salicylate + PMT' detection system using the known energy of the 4th harmonic of 1064 nm radiation generated in the nonlinear crystals. This allowed calibration of the monochromator at a wavelength of 266 nm. Since the quantum yield of sodium salicylate is equal in a broad spectral range between 40 and 350 nm, calibration of the registration system at 266 nm allowed calculation of the conversion efficiency for the higher harmonics. The monochromator allowed observation of the harmonics down to a spectral range of 50 nm. The conversion efficiency in the plateau range (15th–21st harmonics) was measured to be in the range of 10^{-6} – 10^{-5}. Table 2.1 summarizes the measured conversion efficiencies for different harmonics in the case of some metal-containing plasma plumes.

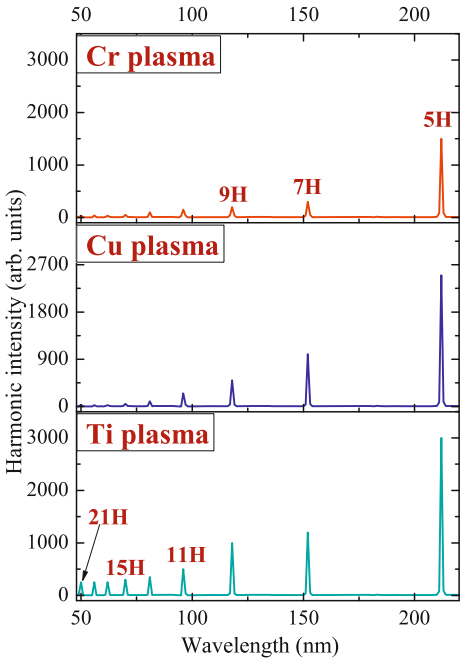

Fig. 2.4 High-order harmonic spectra from the Cr, Cu and Ti plasma plumes. Reproduced from [78] with permission from IOP Publishing

While most of the plasmas demonstrated similar properties, some of them allowed the observation of unusual spectral distributions of harmonics. In particular, in some cases the generation of harmonics was restricted at the 9–15th orders. Among those plasmas were the Al, B and Mo plumes (Fig. 2.5a). A few other plasmas showed even more interesting spectra, where one could distinguish the enhancement of some harmonics with regard to the lower-order ones. These were the In and Nb plasma plumes, which showed enhancement of the 11th harmonics compared with the previous harmonic orders (Fig. 2.5b). Such dependences resemble those observed in previous plasma HHG experiments using 800 nm, few tens of femtosecond pulses in the cases of In, Mn, Cr, Sn and other plasmas [74, 75]. The commonly accepted explanation of these enhancements is related to the closeness of the specific harmonic orders to the resonance ionic transitions of these media. Below we discuss this peculiarity in more detail.

The dependence of the recombination probability on the electron return energy and on the structure of the target is reflected in the HHG spectrum and has been the subject of intensive research in recent years. To enhance the notoriously low efficiency of the HHG process, it appears promising to exploit the effect of resonances, which are known to be of great importance in photoionization. The investigation of resonant peaks in the photoionization cross section has a long history, including studies of autoionising resonances [79], shape resonances [80] and giant resonances [81], but there have been only a few studies on the role of resonances in HHG. The role of

Table 2.1 Harmonic conversion efficiencies ($\times 10^{-6}$) in various plasma plumes

Harmonic order	Wave length, nm	Sn	Zn	Mn	Ti	Cu	W	Au	B	Ta	Ag	Cr	Mo	Al
5	213	100	80	80	70	46	46	40	40	26	20	20	4.2	6
7	152	66	66	20	20	33	40	33	13	10	16	7.1	3.8	2.59
9	118	66	53	10	12	15	38	26	3	3	10	3.8	2.5	1.33
11	97	53	40	6.6	6.6	13	33	20	1.3	1.8	6.6	3.8	2.1	
13	82	26	4	2.1	4.6	2.5	7	1.8	1	0.9	2.6	1.3	0.9	
15	71	16	4	1.75	3.3	0.9	5	1.3		0.9	1.3	0.9		
17	63	6	1.7	1.3	2.1	0.9		1.3		0.9	1	0.9		
19	56	6	1.7	1.3	2.1	0.83		0.9		0.75	1	0.9		
21	51	4	1	1.3	2.1	0.75		0.9		0.75	1	0.9		

Reproduced from [78] with permission from IOP Publishing

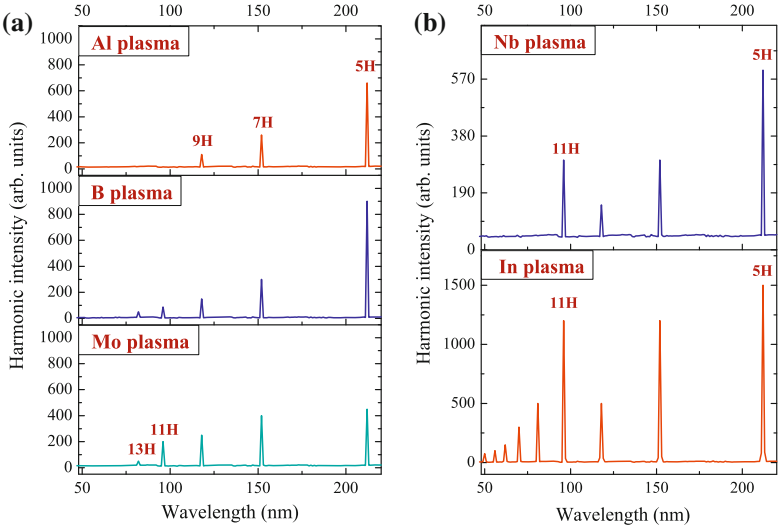

Fig. 2.5 **a** Harmonic spectra from the Al, B, and Mo plasmas producing only low-order harmonics. **b** Harmonic spectra from Nd and In plasmas demonstrating the enhancement of 11th harmonic with regard to the lower-order ones. Reproduced from [78] with permission from IOP Publishing

atomic resonances in increasing the laser radiation conversion efficiency was actively discussed in the framework of perturbation theory in the early stages of the study of low-order harmonic generation (see the monograph [82] and the references therein). In the case of HHG, the increase in the efficiency of the generated harmonics due to resonance processes first came under discussion more than a decade ago, and this approach appears to have considerable promise with the use of ionic and, in some cases, atomic resonances [14, 15, 83–88]. These studies comprised both theoretical treatment of the process and description of the first attempts to form resonance conditions in experiments.

While theoretical estimates testified to the possibility of an efficient enhancement of individual harmonics and groups of harmonics, experimental works revealed the difficulties encountered in HHG in gases. Therefore, the use of plasma media could largely facilitate solution of the problem of resonance harmonic enhancement. Examination of a large group of potential targets allowed identification of some of them as suited for demonstrating this process [75]. The advantages of 'plasma HHG' over 'gas HHG' were amply manifested in this case, because the number of possible media in the former case is far greater than that in the latter case. Some attempts at explanation of the experimental observations of resonant enhancement in plasma harmonics have been reported recently in [89–93].

The observation of resonance enhancement in the case of both femtosecond and picosecond probe pulses is related with the coincidence of harmonic wavelengths and ionic transitions. In the case of femtosecond pulses, this opportunity has more chances to be realized due to the broader bandwidth of the harmonics. However, the conditions of resonance enhancement could be realized in the case of picosecond pulses as well once some of the resonances of Nb and In ions occasionally coincide with the wavelength of the 11th harmonic. These observations were repeated several times during analogous studies of the same plasmas, while none of the other plasma plumes demonstrated these features.

Propagation effects could not explain these observations since in that case we would have to observe the enhancement of at least a few neighboring harmonics as well. One can note that the resonance enhancement of plasma harmonics in the case of narrowband probe pulses is indeed a rarely observed phenomenon. The application of various plumes showed this enhancement only in the two above-mentioned plasmas, while many more plasmas were reported as suitable for resonance enhancement in the case of femtosecond broadband pulses. Overall, Fig. 2.4 shows the tendency of the harmonic distribution, which was common for most of the studied plasma plumes. Figure 2.5 emphasizes the peculiarities of the harmonic distribution observed in some plasma plumes. Those observations showed that the atomic number does not play a significant role in the classification of the harmonic properties of the plasma media. The important parameter here could be a second ionization potential of the species used.

A few properties of the generated harmonics from metal-ablated plasmas were analyzed in depth. The delay between heating and probe pulses is crucial for optimization of the HHG. A typical dependence of the harmonic intensity on the delay between pulses is presented in Fig. 2.6a in the cases of Pb and Mn plasmas. The concentration of particles (neutrals and singly charged ions) is insufficient at the initial stages of plasma formation and spreading out of the target surface, since the species possessing velocities in the range of 5×10^5 cm s^{-1} do not reach the optical axis of propagation of the probe beam (100–150 μm above the target surface). Increase of the delay above 5 ns allowed the appearance of plasma particles along the path of the converting pulse, which led to considerable growth of the HHG conversion efficiency. Further increase of delay led to saturation of the HHG and gradual decrease of the conversion efficiency at longer delays. One can note that there are different optimal delays for the harmonics generated in the Mn and Pb plasmas (20 and 90 ns

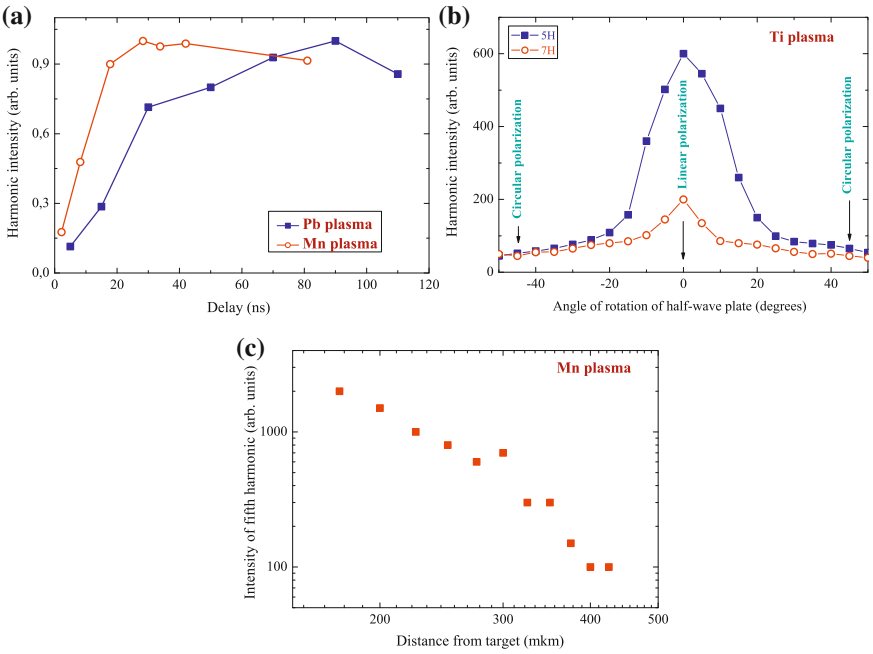

Fig. 2.6 **a** The dependence of the harmonic intensity on the delay between the heating and probe pulses for the Pb and Mn plasmas. **b** The polarization dependences of the 5th and 7th harmonic intensities at different angles of rotation of the half-wave plate in the case of the Ti plasma. **c** The harmonic intensity as a function of the distance between the target surface and the probe beam axis for the 5th harmonic generated in Mn plasma. Reproduced from [78] with permission from IOP Publishing

correspondingly). These observations can be explained by the different velocities of the ablated particles from these targets, which should reach the area of interaction with the probe pulses at different times. In this connection the application of a heavy target (Pb, $Z = 82$) should lead to a longer delay before the bulk amount of ablated material interacts with probe beam compared with a lighter target (Mn, $Z = 25$). The ratio between optimal delays for these plasma samples is approximately coincide with the ratio between the masses of those particles, which should follow from the equal kinetic energies of ablated particles.

Usually, the plasma lifetime is of the order of a few nanoseconds [94]. However, one should consider as another parameter the time when the maximum concentration of particles appears above the target surface in the area of propagation of the driving laser pulse. Since the distance from the target to the axis of the driving pulse propagation is of the order of 100–150 μm, the time when the main cloud of particles reaches this area is of the order of a few tens of nanoseconds and is defined by the velocity of the particles ($\sim 5 \times 10^3$ m s^{-1} for the targets with low Z and $\sim 2 \times 10^3$ m s^{-1} for the targets with high Z). This time is of the order of 20 or 50 ns. So the meaning of the lifetime is incorrect once we consider the process, which depends only

on the time required for spreading of the plasma particles towards the area where the driving pulse propagates. In particular, the experiments [68] using nanosecond pulses were optimized at 600 ns delay due to a longer distance from the target to the driving nanosecond pulse (∼1 mm). The above estimates allow us to conclude that it is the plasma spreading time, which is more critical than the plasma lifetime. During the plasma HHG the driving pulse interacts with the ion or the atom, because the spreading time is longer than the plasma lifetime.

The important parameter of plasma HHG is the polarization of the probe radiation. Figure 2.6b shows the dependences of the 5 and 7th harmonics generated from the Ti plasma at different angles of rotation of the half-wave plate, which caused variation of the conditions of the driving radiation from linear (at 0°) to circular (at 45°) polarization. A small deviation from linear polarization led to a considerable decrease of the 5 and 7th harmonic intensities, which is typical behavior for high-order harmonics. The application of circularly polarized laser pulses led to complete disappearance of harmonic emission, as should occur assuming the origin of HHG.

The harmonic intensity also considerably depended on the distance between the optical axis of the driving beam and the target surface (Fig. 2.6c). This dependence is induced by the change of plasma concentration above the target. The log–log dependence of the harmonic intensity (I_h) on the distance between the optical axis of the driving beam and the target surface (x) for the 7th harmonic generation in manganese plasma corresponded to $I_h \sim x^{-3.5}$.

We would like to recall that the earliest observations of HHG in gases were also reported using a picosecond Nd:YAG laser [95, 96] (as well as an excimer laser at 248 nm [97]). The harmonics from different gases up to the 21st and 33rd orders of 1064 nm radiation were reported at an intensity of 3×10^{13} W cm^{-2}, which led to an enormous growth of interest in this area of nonlinear optics. The present studies demonstrate that the application of ablated plasma as a nonlinear medium can further amend this HHG technique using picosecond driving pulses, once the metal atoms, ions and clusters become involved as efficient sources of harmonic generation.

2.3 Stable Generation of High-Order Harmonics of Femtosecond Laser Radiation from Laser Produced Plasma Plumes at 1 kHz Pulse Repetition Rate

Almost all HHG studies from weakly ionised plasmas produced during laser ablation of various solid targets were carried out using the 10 Hz pulse repetition rate lasers. Up to now only few studies of HHG from plasmas have been carried out on static targets using 1 kHz class lasers. The ablation process at 1 kHz pulse repetition rate causes a considerable change of the surface properties of the target due to the melting, which deteriorates the plasma plume conditions during laser ablation. Surface degradation of a static target results in an unstable harmonic signal so that movement of the target surface is required to maintain a reasonable stability. The demand in finding

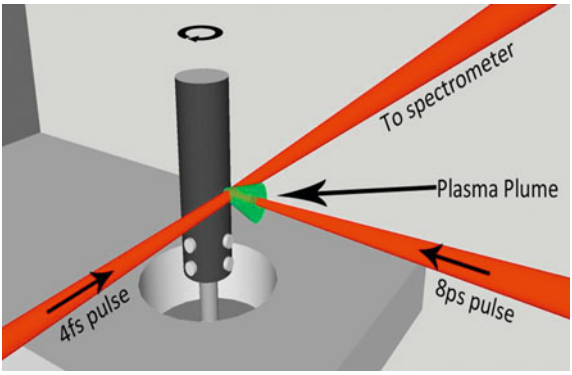

Fig. 2.7 Schematic of the rotating target and HHG configuration. Reproduced from [73] with permission from Optical Society of America

the optimal way for improving the plasma harmonic stability is high due to recent observations of the advanced properties of plasma harmonics over gas harmonics [61, 62, 66]. In particular, in [61], the plasma HHG conversion efficiency was measured one order of magnitude stronger compared with gas HHG efficiency. Analogous features were reported in [66].

The obstacle of all plasma harmonic experiments during earlier studies was an insufficient stability of plasma parameters (density, ion and free electron concentrations, excitation conditions, etc.), which led to the instability of harmonic yield and fast decay of harmonic efficiency during irradiation of the same spot of ablating target. As it was mentioned, most of those early studies were performed using a 10 Hz class lasers. Even at this relatively low pulse repetition rate, the stability of harmonics deteriorated after a few hundred shots on the same spot of the surface and even quicker for powder-like materials (fullerenes, nanotubes, metal nanoparticles, various organic and non-organic powders). One can note that laser ablation of those samples can be considered as an important tool for their structural studies using XUV nonlinear spectroscopy.

The application of soft ablation allows the use of the same target for a much longer period than in the case of earlier studies of over-excited targets during laser ablation. Thus a search of a robust, easy-to-apply method for improving the harmonic stability in the case of plasma HHG could considerably advance a search of the fundamental (structural, orientational, etc.) properties of organic and inorganic atoms and molecules through XUV nonlinear spectroscopy.

The earlier used approaches of a rotating disc geometry [20, 98] are not suitable since the distance between driving femtosecond beam and target surface should be maintained minimal (of order of 100 μm), while the Rayleigh length of the driving beam is maintained at the range of few mm. Below we describe a new method using a motorized rotating rod specifically prepared for the HHG from plasma plumes using high pulse repetition rate lasers, and demonstrate that this target significantly improves the stability of high-order harmonics [73].

Those studies were performed using two laser pulses: one to create the plasma plume and the second to drive the HHG within it. The first (heating) pulse was

created by splitting off a portion (200 μJ) of the uncompressed 8 ps laser pulse from a 1 kHz Ti:sapphire chirped pulse amplification laser. The remaining driving pulse was compressed in a prism compressor and then further compressed using a hollow core fibre and chirped mirrors, resulting in 250 μJ, 4 fs pulses. The driving pulse was delayed with respect to the ablation pulse by 35 ns to give the plasma the time to expand away from the target surface to allow the converting pulse to pass through the plasma without being clipped by the target.

Target rotation apparatus consists of three linear stages driven by stepper motors along three axes. The target was attached to an axis of the fourth motor, which provided rotation with a variable speed (from a few rotations per minute (rpm) up to 300 rpm). Rotating the target was sufficient to achieve stable harmonic radiation and an additional vertical movement was not required, though this capability might be useful for future plasma HHG experiments. As the setup requires the target to be positioned very close to the driving beam, it was of paramount importance that the target was carefully aligned to the axis of rotation. Any movement of the target surface due to eccentricity in the radial direction from the driving beam axis would result in an oscillation of the harmonic signal due to variation of the plasma density seen by the driving beam or, in the extreme case, clipping of the laser beam.

The target (cylindrical rode with diameter of 10 mm and length of 30 mm) was positioned as shown in Fig. 2.7, with the probe pulse propagating $100 - 200\,\mu m$ above the target surface. The picosecond heating pulse was focused onto the surface of the rotating target. In order to efficiently produce high harmonics the plasma must be weakly ionised [75]. To achieve this the target was positioned slightly in front of the focus of the heating pulse using a 50 cm focusing lens, leading to an on target intensity of $\sim 1 \times 10^{10}\,W\,cm^{-2}$. This also had the benefit of increasing the size of the plasma produced from ablating a larger area. The size of the focus at the target surface was measured to be ≈500 μm. The delayed probe pulse was focused through the plasma using a 40 cm spherical mirror. The HHG radiation was analysed by an XUV spectrometer consisting of a flat-field grating and an imaging microchannel plate detector with phosphor screen imaged onto a CCD camera.

Figure 2.8 shows that there is a drastic change in the harmonic signal (integrated over the spectral range of 40–80 nm) when the rotation of the aluminium target is stopped. There is a sharp intensity decrease of more than one order of magnitude over only one thousand shots (or just after one second of ablation using 1 kHz laser). The benefits of the rotating rod are clearly shown in Fig. 2.9a where stable harmonic generation was achieved from the plasma produced on an aluminium target for over 1 million laser shots. Figure 2.9b shows the sharp increase and slow decay in the HHG from silver plasma when the target is moved vertically by one millimetre after about 6×10^5 shots. This caused a quick increase in the harmonic signal from the fresh surface, followed by further decay down to the stable level. The decaying behaviour disappears as the laser creates a rotationally precise micro-channel on the target surface. The reason for the degradation of harmonic signal is clearly due to effects on the surface of the target. Stable harmonics were achieved in a broad range of the speeds of rotation (from 10 rpm and faster). The target rotational speed and the size of the ablation focus imply that the same area of target was undoubtedly used

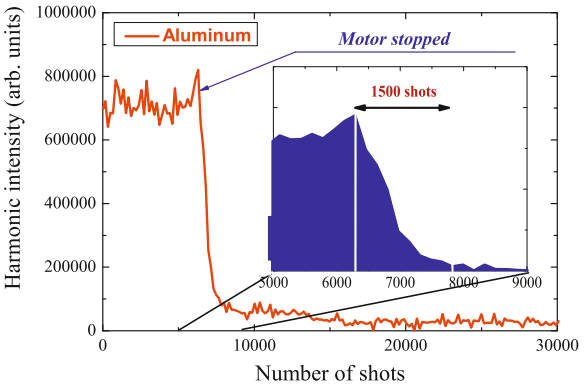

Fig. 2.8 Decay of the harmonics from aluminium plasma after stopping the rotation of the motor. The harmonics were integrated over 40–80 nm spectral range. Reproduced from [73] with permission from Optical Society of America

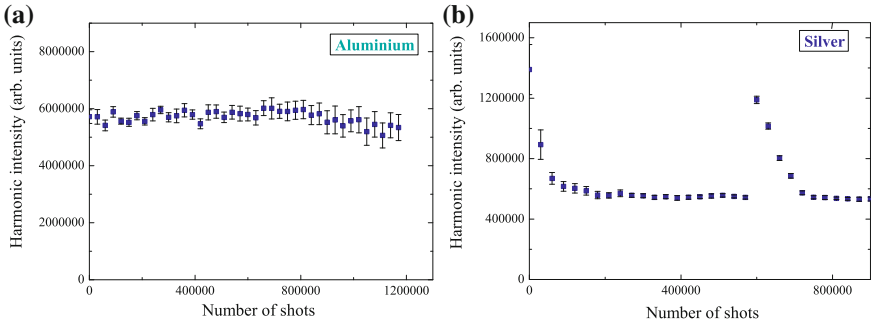

Fig. 2.9 Stability of integrated harmonic signal from (**a**) aluminium and (**b**) silver plasmas. Reproduced from [73] with permission from Optical Society of America

repeatedly for consecutive rotations over the 20 min duration of experiments. This could result in thermal damage issues with this high pulse repetition rate.

It is possible that once the fixed surface is melted the force from a following laser shot and plasma creation could expel some of the liquid target from the ablation area creating a deeper hole out of the focus or with angled side, which would not cause the plasma to be emitted in a direction normal to the surface. These effects are considerably diminished once the target starts to rotate. During rotation, the previously ablated area cools down such that, during the next set of ablation on this spot, the plasma formation occurs at approximately same conditions. To prove that the ablated area cools down with rotation, the target was rotated at different speeds (from 10 to 300 rpm) and no difference in stability of harmonic yield was found. These observations point out the importance of the periodic change of the ablation zone. This also confirms a suggestion that the cooling of the ablation area leads to stable plasma generation.

Characteristics of plasma (density and ionisation state) are the most important parameters to achieve and maintain stable HHG efficiency during an extended period of illumination. The calculations [66] have shown that, in the case of carbon plasma, the concentration of particles in the area of femtosecond laser-plasma interaction at optimal delay between heating and driving pulses (~40 ns) is $\sim 2 \times 10^{18}$ cm^{-3}. The solid surface was considered as the one unheated before the laser ablation. Indeed, after one round of rotation (e.g., after 0.2–2 s), the plasma disappears, the ablated spot cools down, and the next laser shot on the same spot can be considered as a shot on the "fresh" surface. Contrary, in the case of a stationary target, the following shots continue the heating of the same spot.

The novelty of this approach includes the observation of advanced properties of plasma HHG even at extremely small energies of the heating pulses. The efficiency of plasma HHG depends on the possibility to create "optimal" plasma. This can be done using both multi-mJ pulses, as was shown in previous studies [75], and few hundred μJ pulses, as it was demonstrated in the reviewed work [73] and recently published studies [66]. The important point here is the intensity and fluence of the heating pulse on the target surface. The application of a higher energy heating pulse could create the conditions of "optimal" plasma over a longer distance, which could (or could not) increase the harmonic yield depending on the phase relations between the driving and harmonic waves. In addition, it can also lead to the over-heating of the target at 1 kHz ablation. As it was already mentioned above, the rotating speed did not influence the stability of harmonics using 0.2 mJ heating pulses. The use of more energetic pulses at high repetition rate (i.e. of order of few mJ) may require additional optimisation of the rotation target technique (for example, by periodic up and down dragging of the rotating target).

2.4 High-Order Harmonic Generation in Graphite Plasma Plumes Using Ultrashort Laser Pulses: A Systematic Analysis of Harmonic Radiation and Plasma Conditions

The characteristics of laser plasma play a crucial role in determining how efficiently high harmonics can be generated in the plasma plumes. An increase in the free electron density was likely to have been the limiting factor for the harmonic cut-off energy in early experiments with laser plasmas [17, 19, 20]. A search for appropriate target materials, which can provide favourable ablation plasmas for efficient HHG, has motivated the analysis of plasma characteristics at conditions of high harmonic yield. Recent studies have shown that carbon ablation plasmas are promising media to satisfy the above requirements [61–63, 66].

Shot-to-shot stability of the harmonic signal is crucial for any application of the generated radiation and especially for the measurement of the pulse duration of converted XUV radiation. Such temporal measurements were reported in the case of HHG in chromium plasma [61]. Using the "Reconstruction of Attosecond Beating

by Interference of Two-photon Transitions" technique [99], the authors have shown that the 11th to the 19th harmonics of a Ti:sapphire laser form, in the time domain, an attosecond pulse train. It was underlined that instability of the harmonic signal in their experiments using a 10 Hz pulse repetition rate laser was the main obstacle for an accurate measurement of the temporal structure of plasma harmonics. Beside its fundamental interest, high-order harmonic generation in plasma plumes could thus provide an intense source of femtosecond and attosecond pulses for various applications.

Optical parametric amplifiers (OPAs) operating in the mid-infrared (MIR) range are promising tools for harmonic cut-off extension and attoscience experiments. The spectral cut-off energy of HHG obeys the scaling law $E_c \sim I\lambda^2$ [23], where I is the peak intensity of the probe field and λ its central wavelength, which allows one to extend the harmonic emission beyond the 100 eV range by using longer wavelength laser sources. Another advantage of mid-infrared optical parametric amplifiers (MIR OPAs) is their wavelength tuneability, which allows one to tune the spectral position of harmonics towards the ionic transitions with strong oscillator strengths. This feature allows the observation of resonance-enhanced harmonics and broadens the range of plasma samples where this phenomenon could be realized compared with the case of ~800-nm lasers of essentially fixed wavelength [69]. Moreover, by using two-colour HHG techniques, the application of MIR OPAs allows the study of complex molecules during their ablation and HHG using the tuneable long-wavelength radiation. These features are interesting for spectroscopic applications of HHG in the MIR range [100, 101].

In the meantime, the use of MIR OPAs for HHG should lead to a reduced harmonic generation efficiency that scales as λ^{-5} [102, 103]. It is of considerable interest to analyse the relative behaviour of plasma harmonics in the cases of 800 nm and MIR lasers and thereby to find the conditions when the reduction of harmonic yield becomes not so dramatic due to some enhancement mechanisms, such as the presence of in-situ produced nanoparticles, which increase the HHG conversion efficiency. It is worth noting that previous studies of plasma HHG in carbon plumes [61, 62] have inferred, through analysis of plasma debris morphology, the formation of nanoparticles during laser ablation of carbon-contained targets.

Atomic carbon is a reactive species, which stabilizes in various multi-atomic structures with different molecular configurations (allotropes). All the allotropic forms of carbon (graphite, diamond, and amorphous carbon) are solids under normal conditions, but graphite has the highest thermodynamic stability. Laser ablation of graphite has been intensively examined during the last ten years to define plasma conditions for the synthesis of carbon structures with unique properties. The physical characteristics of the plasma plume, such as concentration of atoms and clusters, directly affect the properties of the material being formed in the dynamic expansion of the ablated material. The successful synthesis of clusters is strongly dependent on the formation of atomic and molecular species with the required chemistry and aggregation ability. Thus, to select the optimal plasma conditions for HHG, a detailed understanding of the basic physical processes governing the ablation plume composition and reliable methods for controlling of the plume species are needed. The reasons mentioned

above and the consideration of recent studies of HHG in carbon plasmas [61, 62], as well as recently reported comparisons of the HHG in graphite-ablated plasmas and argon gas [63, 66], have prompted to systematically analyze the plasma conditions for optimal HHG conversion efficiency in graphite plasmas [104].

2.4.1 HHG in Carbon Plasma at Different Conditions

High-intensity few-cycle pulses (760 nm central wavelength, 0.2 mJ, 3.5 fs, pulse repetition rate 1 kHz) were typically obtained from the Ti:sapphire laser after second stage of compression consisting on hollow fiber filled with neon and bunch of chirped mirrors [105]. The compressed pulses were characterized with a spatially encoded arrangement for direct electric field reconstruction by spectral shearing interferometry. This radiation was used for frequency up-conversion in the specially prepared carbon plasma.

A portion of the uncompressed radiation of this laser (central wavelength 780 nm, pulse energy 120 μJ, pulse duration 8 ps, pulse repetition rate 1 kHz) was split from the beam line prior to the laser compressor stage and was focused into the vacuum chamber to heat the graphite target and create a plasma on its surface (Fig. 2.10). These picosecond heating pulses were focused by a 400 mm focal length lens and created a plasma plume with a diameter of ~0.5 mm using an intensity on the target surface of $I_{ps} = 2 \times 10^{10}$ W cm^{-2}. The delay between plasma initiation and femtosecond pulse propagation was fixed at 33 ns. As an alternative ablation, the 10 ns, 1064 nm pulses from a 10 Hz repetition rate Q-switched Nd:YAG laser were used that provided an intensity on the target surface of 1×10^9 W cm^{-2}. In that case the delay between the 10 ns heating pulses and the 3.5 fs probe pulses was varied in the range of 10–60 ns to maximize the harmonic yield.

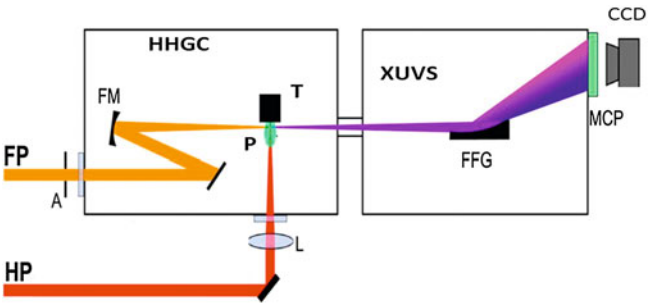

Fig. 2.10 Experimental setup for harmonic generation in plasma plumes. *FP* femtosecond probe pulse, *HP* picosecond heating pulse, *A* aperture, *HHGC* high-order harmonic generation chamber, *FM* focusing mirror, *L* focusing lens, *T* target, *P* plasma, *XUVS* extreme ultraviolet spectrometer, *FFG* flat field grating, *MCP* microchannel plate and phosphor screen detector, *CCD* CCD camera. Reproduced from [104] with permission from IOP Publishing

The 3.5 fs probe pulses, propagating in a direction orthogonal to that of the heating pulse, were focused into the laser plasma using a 400 mm focal length reflective mirror. The position of the focus with respect to the plasma area was chosen to maximize the harmonic signal, and the intensity of femtosecond pulses at the plasma area at these conditions was estimated to be $I_{fs} = 6 \times 10^{14}\,W\,cm^{-2}$. The 30 fs, 780 nm, 2 mJ probe pulses from another Ti:sapphire laser operating at 1 kHz repetition rate and producing approximately the same intensity inside the laser plasma were also used for HHG. The details of this setup and registration system are presented in [66, 70].

In order to analyse the harmonic yield of the MIR source in the graphite-ablated plasma an OPA pumped by the 30 fs Ti:sapphire laser was used. A beam splitter inserted before the laser compressor of this Ti:sapphire laser allowed to pick off 10 % of the beam (780 nm, 1 mJ, 160 ps, 1 kHz pulses) to generate a plasma plume on the graphite targets, with the remaining 90 % being compressed to 30 fs (7 mJ) to pump a commercial OPA. The OPA was optimised for high conversion efficiency, beam quality and duration of the converted pulses. To achieve high reproducibility of the generated pulses, all the amplification stages were driven to saturation. This device generated 35 fs signal pulses in the 1200–1600 nm range. The idler pulse covered the 1600–2200 nm range. The delay between the heating ablation pulse and MIR pulses from the OPA was set to 35 ns, as this delay was found to be optimal for the efficient generation of extended harmonics.

Since the goal of these studies was to analyse the graphite ablation plasma characteristics at the conditions of efficient HHG of ultrashort laser pulses, this process was firstly optimised by achieving the maximum conversion efficiency and highest harmonic cut-off using the probe radiation from both Ti: sapphire lasers with fixed wavelengths and the tuneable OPA. Then the efforts were concentrated on the analysis of the "optimal" plasma plume using three techniques: optical emission spectroscopy of emitting plasma species in the visible, UV and XUV spectral ranges; scanning electron microscopy for inspection of the deposited plasma debris; and finally time-of-flight mass spectrometry for analysis of the ionic components of the plasma.

To analyse the influence of the spectro-temporal characteristics of the probe radiation on the harmonic yield, the backing pressure of neon in the hollow fiber of second compressor was changed, which allowed the variation of pulse duration from 25 to 3.5 fs [106]. The dependence of the spectral and intensity characteristics of the harmonic images recorded by the CCD camera in the 15–25 eV range at different input pulse spectra and backing pressures of neon are shown in Fig. 2.11. One can clearly see that, with the increase of backing pressure (from 1.2 to 3 bar), the harmonic intensity increases, while the harmonic wavelength spectrally shifts towards the blue. During these experiments the driving pulse energy was held constant.

An interesting feature of the carbon harmonic spectrum from the 10 ns pulse-induced plasma is that the spectral width is about 2–3 times broader than that of harmonics generated in other atom- and ion-rich plasmas at the same fluence and intensity of heating pulse, when using few-cycle pulses. For example, the full width at half maximum for medium-order harmonics was 1.5 nm in the case of graphite

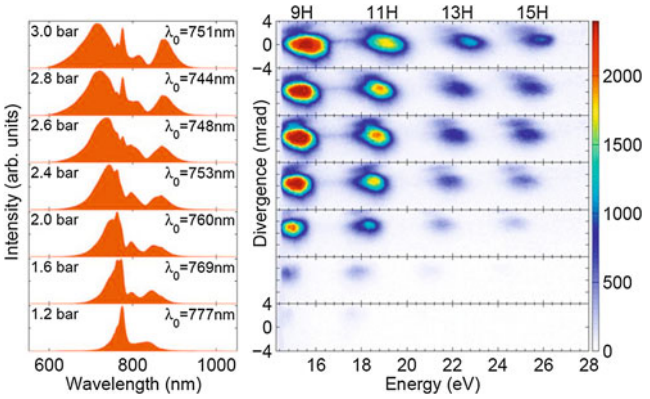

Fig. 2.11 Carbon harmonic spectra as a function of neon pressure in the hollow fiber. The corresponding laser spectra measured in front of the vacuum chamber are presented on the *left* side. The plasma was created using the 10 ns pulses. λ_0 is the central weighted wavelength of the spectral distribution. The colour scale indicates the harmonic intensity. Reproduced from [104] with permission from IOP Publishing

plasma, versus 0.4 nm for different metal (Ag, Al, and Cu) plasmas. The broader width of the harmonics can be explained by self-phase modulation and chirping of the fundamental radiation propagating through the carbon plasma. The presence of nanoparticles in the plasma plume may also contribute to bandwidth broadening of harmonics.

For practical applications of the coherent short-wave radiation generated in graphite plasma using a 1 kHz driving laser, it is necessary to analyse the stability of the plasma characteristics and the generated harmonics. Recently introduced new technique for maintaining a stable ablation plasma for harmonic generation using high pulse repetition rate lasers (1 kHz) based on a cylindrical rotating metal target [73] was described in the previous section. The studies [104] have shown that, in spite of the different properties of metal and graphite targets, the rotating target allowed achieving stable HHG in both metal and graphite plasmas. Figures 2.12a,b show the improved stability over $\sim 10^6$ laser shots of the 11–25th harmonics when using a rotating graphite target and how the harmonic intensity rapidly decays after the target rotation is stopped. The rotating graphite rod allows maintaining a relatively stable harmonic yield well above 1×10^6 laser shots. Harmonics up to the 29th order were routinely observed in these studies using the 3.5 fs pulses.

It is worth noting that harmonic intensity is the same when returning to the same spot after one rotation of the graphite rod. This reveals the unchanged morphological target conditions. Indeed, target analysis by optical inspection has confirmed that there is negligible surface modification due to laser ablation provided the ablation spot continuously moves along the target surface. This means that in graphite, like in metals, under repetitive ablation on the same target position at 1 kHz, the instability of the plasma and generated harmonics is largely related with the unstable conditions

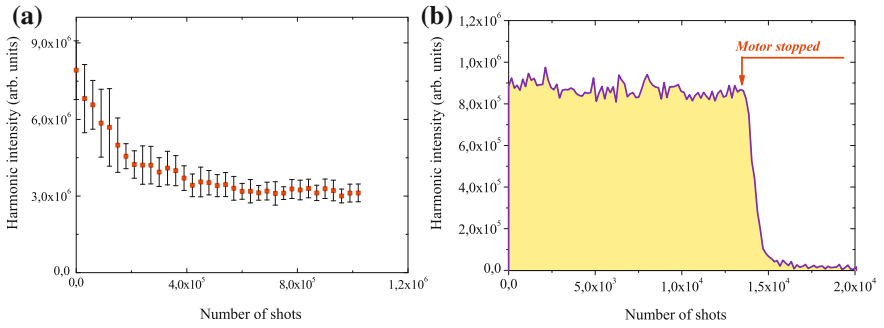

Fig. 2.12 Harmonic generation in graphite plasma using 3.5 fs pulses. **a** Stability of harmonic intensity over 1 million shots on a graphite target integrated over the 11–25th harmonics. **b** Decay of harmonics after stopping the motor rotating the target. Reproduced from [104] with permission from IOP Publishing

of the ablating spot. After moving to a new spot, the previous irradiated target area cools down and becomes again available (one rotation later) for further ablation with the same harmonic output, as in the case of metal rods. Therefore using a rotating graphite rod can significantly improve the stability of the harmonic signal.

Upper panel of Fig. 2.13 shows the harmonic spectrum generated in the case of 1300 nm probe pulses. Harmonics up to the 57th order were observed at the conditions of carbon plasma formation using the heating uncompressed 160 ps pulses from this laser. It is worth noting that application of less intense 1400 nm pulses available by tuning the OPA, while generating weaker harmonics, did not result in a higher harmonic cut-off than in the case of 1300 nm. This observation suggests that the harmonic generation occurred under saturated conditions, with the expectation of even stronger harmonics once the micro- and macro-processes governing frequency conversion are optimised.

Harmonic spectra up to the 29th order in the case of 780 nm, 30 fs probe pulses, are presented in the bottom panel of Fig. 2.13. By comparing with the spectra collected with the 1300 nm driving source (same figure, upper panel), one can clearly see the expected extension of harmonic cut-off in the case of the longer-wavelength driving source. The important peculiarities of these comparative studies are the broadband harmonic spectra in the case of 1300 nm laser and the similar yield of harmonics at the two driving wavelengths. Whilst the former feature depends on the bandwidth of the OPA output, the later observation requires additional consideration. The plasma harmonic yield from the MIR source did not follow the expected $I_h \propto \lambda^{-5}$ rule. In fact, for the intensities of MIR and 780 nm pulses used ($\sim (2\text{–}4)\times 10^{14}\,\mathrm{W\,cm^{-2}}$), the harmonic efficiency of the XUV radiation driven by MIR pulses was higher compared with the case of 780 nm pulses, assuming lower energy of the former pulses (0.2 and 0.54 mJ respectively). One can note that the $I_h \propto \lambda^{-5}$ rule predicts a ~13-fold decrease of conversion efficiency for the MIR (1300 nm) pulses compared with the 780 nm pulses at equal probe pulse intensity.

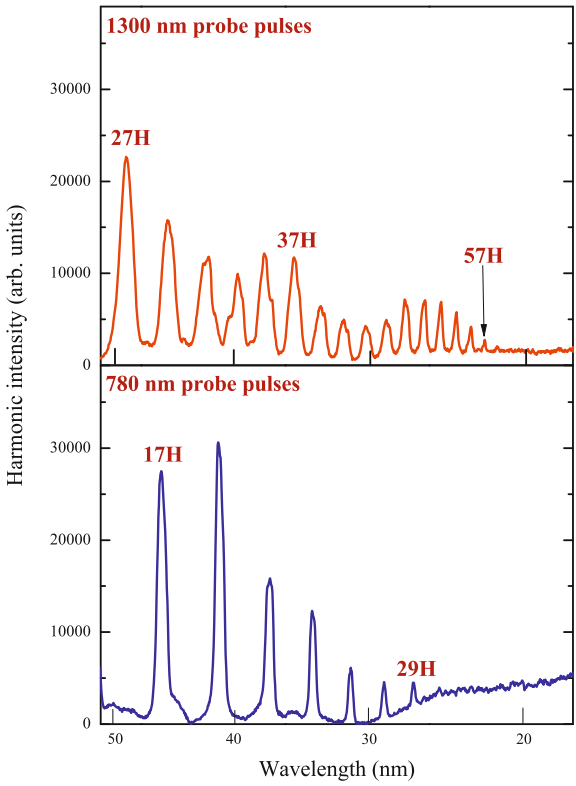

Fig. 2.13 Plasma harmonic spectra using the 1300 nm (*upper panel*) and 780 nm (*bottom panel*) probe pulses. The energies of probe pulses were 0.2 mJ (*upper panel*) and 0.54 mJ (*bottom panel*). Ablation was carried out using 160 ps, 780 nm, 1 kHz laser pulses. Reproduced from [104] with permission from IOP Publishing

2.4.2 Characterization of Optimal Plasma Conditions

This section presents the characterization of the graphite ablation plasma plumes at conditions of maximum HHG conversion efficiency. In graphite, the ablation plasma plume may contain various species of carbon, i.e. neutrals and ions, small molecules, clusters, aggregates, etc., which can contribute to harmonic generation in various extents. It is important to determine their presence in the region where the driving laser pulse interacts with the expanding plasma. In particular, the production of clusters in the laser plasma during laser ablation of various targets has a high probability, while their presence and concentration in the plasma area where the frequency conversion occurs is yet to be confirmed directly. Another issue is how one can define the density of monomers, dimers and clusters and their influence on the HHG yield. Analysis of post-ablation conditions of the deposited debris can provide information on the nature of the nonlinear species, despite the differences between the composition of the plasma in its early stages and the deposited material, due to the influence of conditions of aggregation on the substrate [107]. Another issue of interest is whether the spectral characterisation of the plasma emission in the visible and UV ranges can

provide some clues about the plasma conditions, without the simultaneous analysis of the XUV emission.

Plasma characterization through optical spectroscopic measurements in the visible, UV, and XUV ranges at the conditions of different HHG efficiencies were carried out using the above-described XUV spectrometer and a fiber spectrometer. The fluences of heating pulses at which the spectra were recorded corresponded both to optimal and non-optimal conditions of HHG. The acquisition times were set to 1 s, for measurements of XUV spectra, and to 0.5 s, for measurements of visible and UV spectra. Characterisation of the plasma debris collected on silicon wafers placed 4 cm from the ablated target was carried by scanning electron microscopy (SEM).

Cluster composition of the ablation plume produced by nanosecond laser pulses was investigated by time-of-flight mass spectrometry (TOFMS). A brief description of the experimental set up is given here; more details of the TOFMS can be found elsewhere [108]. The laser beam (1064 nm, 5 mJ, 10 ns pulse duration) was focused at normal incidence to a 0.2 mm spot on the surface of the graphite target. The laser intensity was 1.5×10^9 W cm^{-2}, which resulted in the creation of an optimal plasma for efficient HHG using the nanosecond ablation pulses. The target was placed in a vacuum chamber (pumped to $\sim 2 \times 10^{-6}$ bar) between the extracting and accelerating plates of a linear TOFMS. The target surface was parallel to the flight axis of the spectrometer. The target could be rotated and displaced at variable distances from the axis. Positive ions produced in the ablation were deflected along the TOFMS axis by an electric field typically in the range of 300−400 V cm^{-1} and accelerated by a total voltage of 2500 V. A high voltage switch was used to apply the bias voltage at controlled delays with respect to the laser ablation pulse. Ions entered the drift region (flight length ∼1 m) and were detected by a microchannel plate. Analysis of neutral species produced in the ablation could also be performed by the use of a second post-ionization laser (F_2 excimer at 157 nm). The post-ionization laser pulse interacted with the ablation plume perpendicularly to the plume propagation axis, at different distances from the target surface and at different delays with respect to the ablation laser.

It has been shown previously that efficient harmonic emission is observed only in the case when the visible and UV plasma emission is dominated by neutral and singly ionized carbon lines [67]. The studies [104] have also confirmed this feature at the laser fluence used to heat the target surface (Fig. 2.14a). The broad features near 470, 515, and 555 nm could be assigned to the bands of excited C_2 molecules. These bands have also been observed early studies of the ablation of graphite (see for instance [109–111]). Other lines in the spectra presented in Fig. 2.12a are attributed to the neutral and singly charged carbon.

The analysis of optical spectra in the visible and UV ranges does not provide information about the presence of highly ionised species, which can be revealed by collecting the plasma emission in the XUV range. The XUV spectrum of carbon plasmas (Fig. 2.14b) collected following excitation by a 8 ps heating pulse at high intensity, without further excitation by the probe pulse, provides some insight into the plasma components prior to interaction with the driving radiation. This spectrum was collected under conditions of considerable decrease in the nonlinear optical

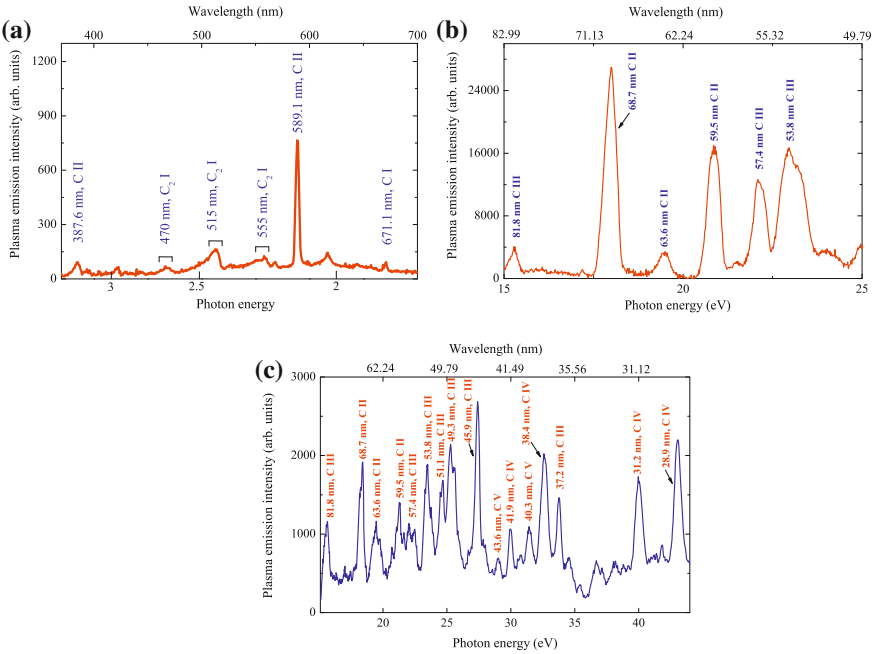

Fig. 2.14 **a** Carbon plasma emission spectrum in the visible and UV ranges at optimal excitation of a graphite target by 8 ps heating pulses (2×10^{10} W cm^{-2}). **b** Spectrum of carbon plasma in the XUV range at over-excitation of the target by 8 ps pulses (5×10^{10} W cm^{-2}). **c** Spectrum of carbon plasma in the XUV range at over-excitation of the target by 10 ns pulses (3×10^{9} W cm^{-2}). Reproduced from [104] with permission from IOP Publishing

response of the medium (i.e. plasma conditions unoptimized for HHG) and revealed the appearance of many emission lines from C II and C III ions. Over-excitation of the target by 10 ns pulses also led to the appearance of emissions from high-charged (C III, C IV) ions (Fig. 2.14c).

It may be noted that these measurements were time-integrated, so one could not say exactly which plasma components existed at the moment of the propagation of the femtosecond beam through the plume. However, the presence of ionic lines from multi-charged species in the last two cases (Figs. 2.14b,c) gives a strong indication of over-excitation of the target and of its negative influence on HHG efficiency. One can note that, at this level of excitation of the graphite plasma, harmonic generation was partially or entirely suppressed. Specifically, a two-fold increase in the intensity of 8 ps pulses (from 2×10^{10} to 4×10^{10} W cm^{-2}) led to a decrease of harmonic intensity by a factor of 2.5. The same can be said about the excitation using longer (10 ns) pulses, though the threshold, at which harmonics started to decay, was considerably lower (2×10^{9} W cm^{-2}). Application of 10 ns pulses with an intensity of 3×10^{9} W cm^{-2} led to a substantial decrease of harmonic efficiency and to the appearance of emission lines from high-charged ionic species (Fig. 2.14c). One

can note that, under conditions of efficient HHG, no ion lines appear alongside the harmonic spectra.

To prove the presence of clusters in carbon plasmas under optimal conditions of harmonic generation, the morphology of deposited debris from the graphite-ablated plasma was analysed during ablation using the picosecond and nanosecond pulses. It has already been mentioned that laser ablation of a solid material is a widely accepted technique for the generation of nanoparticles. However, this process has previously been studied without taking into account the role of free electrons and highly excited ions, which destroy the optimal conditions for phase-matched HHG. SEM measurements of the deposited debris were carried out at the laser ablation conditions corresponding to optimal plasma formation for efficient HHG. The substrates (glass plates and silicon wafers) used to collect the deposited material were placed at a distance of 40 mm in front of the ablation area and the debris was further analysed by SEM.

At optimal plasma conditions, when the highest harmonic conversion efficiency from the carbon-containing 8 ps pulses was measured, the SEM images did not reveal the presence of nanoparticles in the deposited debris with sizes above the limit of detection (10 nm) of the microscope (Fig. 2.15a). This was probably due to the small fluence ($0.2\,\mathrm{J\,cm^{-2}}$) of the heating radiation on the target surface ($I_{ps} = 2.5 \times 10^{10}\,\mathrm{W\,cm^{-2}}$). It is possible that in the case of the carbon plasmas produced at these conditions, harmonics could also originate from nanoparticles with sizes below the limit of detection. Another pattern was observed upon ablation of the target with 10 ns pulses, where considerably higher heating fluence ($10\,\mathrm{J\,cm^{-2}}$) caused the appearance of nanoparticles on a nearby substrate. At relatively moderate conditions of ablation using 10 ns pulses ($I_{ns} \approx (1-2) \times 10^9\,\mathrm{W\,cm^{-2}}$), a high density of nanoparticles appeared in the SEM images of the deposits, with sizes mostly distributed in the range between 10 and 200 nm, with a mean size of 50 nm (Fig. 2.15b). One has to reiterate that these debris characteristics were measured at maximum conversion

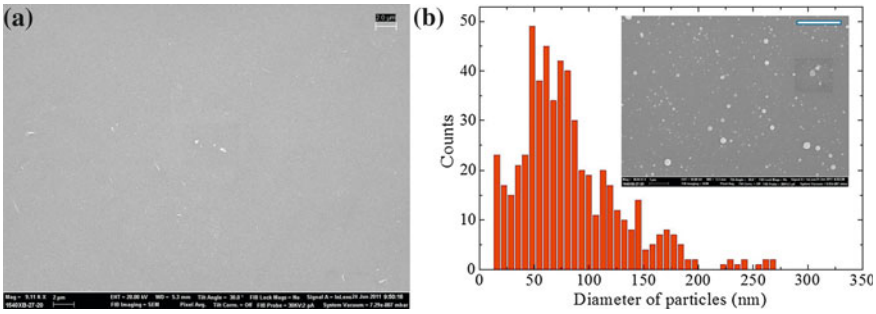

Fig. 2.15 **a** SEM image of the deposited debris after ablation of a graphite target by 8 ps pulses at optimal conditions of HHG. **b** Histogram of size distribution of deposited nanoparticles and corresponding SEM image of deposited debris in the cases of ablation of a graphite target using 10 ns pulses. The size bar on the SEM images is 2 μm. Reproduced from [104] with permission from IOP Publishing

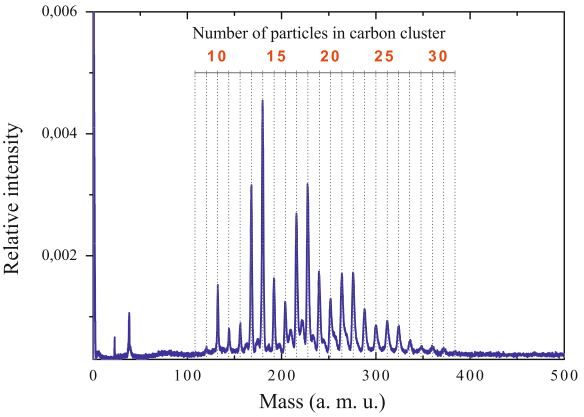

Fig. 2.16 Mass spectrum (in atomic mass units) of carbon plasma obtained during excitation of a graphite target using 10 ns pulses at the conditions close to optimal plasma formation for HHG. Reproduced from [104] with permission from IOP Publishing

efficiency of 15th–23rd harmonics. These morphological studies have confirmed the presence of relatively large nanoparticles deposited on the substrates at conditions of "optimal" ablation using 10 ns pulses. However, some uncertainty still remains about the correlation of these results with the presence of the same nanoparticles in the carbon plasma during harmonic generation, due to the possibility of aggregation of these clusters after deposition. To address this issue, the TOFMS of nanosecond pulse-ablated graphite was carried out.

Figure 2.16 shows the mass-resolved spectrum of carbon plasma after 60 shots of the 10 ns heating pulses. These studies reveal that at plasma conditions close to optimal for HHG, the laser plume contains a group of small, singly ionised carbon clusters (C_{10}–C_{30}). The attempts to find higher mass clusters failed, though the authors of [104] searched for them over a longer range of delays (up to few μs) between the onset of laser ablation and the switching on the triggering pulse in the TOFMS.

To ascertain the presence of neutral species in the ablated plasma, an additional source of ionisation can be used. An F_2 post-ionisation excimer laser ($\lambda = 157$ nm) served that purpose. Photons of this wavelength can induce the ionisation of neutral clusters through single-photon absorption. However, once the 157 nm pulse was focused on the plasma area, no evidence in the mass spectra of neutral clusters was found. This could be explained by the fact that the ionisation potential of carbon ($I_p = 11.2$ eV) is higher than the photon energy of the ionising laser ($E = 7.9$ eV) and by the difficulty of ionising the existing carbon clusters by two-photon absorption of 157 nm radiation, due to low intensity of these pulses in the plasma area.

The concentrations of carbon plasma at the experimental conditions of target ablation (i.e., 2×10^{10} W cm^{-2} in the case of 8 ps pulses and 1×10^{9} W cm^{-2} in the case of 10 ns pulses) allowing efficient harmonic generation were calculated using a

Table 2.2 Calculations of carbon plasma concentration for different intensities of 8 ps and 10 ns pulses heating the graphite target

Intensity, 10^9 W cm^{-2}	Plasma concentration, 10^{17} cm^{-3}	
	8 ps	10 ns
6.6	1.1	
20	2.6	
60	4.0	
0.33		10
1		25
3		37

three-dimensional molecular dynamical simulation of laser ablation of graphite using the molecular dynamics code ITAP IMD [112]. The corresponding concentrations were found to be 2.6×10^{17} cm^{-3} and 2.5×10^{18} cm^{-3}. The results of calculations of carbon plasma concentration for different intensities of heating 8 and 10 ns pulses are summarized in Table 2.2.

2.4.3 Analysis of HHG and Plasma Characterization

A few earlier studies have suggested that the presence of nanoparticles in carbon laser ablation plasmas can explain the observed strong harmonic yield from these media [61, 62]. It was reported that the debris from ablated graphite and carbon lead targets contained nanoparticles with sizes between 100 and 300 nm. The authors of these studies therefore suspected that nanoparticles formed in the plasma by ablation were the source of intense harmonics. Heterogeneous decomposition, liquid phase ejection and fragmentation, homogeneous nucleation and decomposition, and photomechanical ejection are among the processes that can lead to the production and disintegration of nanoparticles [113–115]. A number of different techniques were used in these studies to determine the aggregation state of the evaporated material, including time-resolved emission spectroscopy, CCD camera imaging of the plasma plume, Rayleigh scattering, and laser-induced fluorescence.

In discussed studies [104], SEM for debris analysis and TOFMS were applied for plasma characterization. These two methods have provided useful clues about the conditions and dynamics of plasma plume formed above the target surface. Whilst the former method can provide information about the presence of nanoparticles in the plasma, one has to cautiously consider those results from the following point of view. The deposition process on the substrate happens much later than the time of HHG emission, and the physical process of deposition may lead to further aggregation. Since SEM is an ex-situ method, one cannot exclude the difference between the real composition of clusters in the plasma and the results of SEM measurements, although it clearly proves the presence of clusters in the plasma. TOFMS yields information on the in-situ presence of ionised clusters, although it requires ablation of the target at the same conditions as in the case of HHG experiments and is not well suited for the detection of neutral nanoparticles in the ablated plasma.

TOFMS measurements did not reveal the presence of neutral clusters in the 10 ns pulse produced plasma for the reasons described in the previous section. However, other studies (see for example [110]) have indicated the presence of neutral carbon clusters using two-photon ionisation with an ArF laser (photon energy 6.4 eV). Early TOFMS studies of laser ablation of graphite have revealed the typical characteristics of the expanding plasma species (average velocity $1.5 \times 10^5\,\mathrm{cm\,s^{-1}}$) and their concentration ($4 \times 10^{18} - 6 \times 10^{19}\,\mathrm{cm^{-3}}$ [116]) for ablation with 532 nm, 10 ns pulses at fluences of the order of $3\,\mathrm{J\,cm^{-2}}$. The measured mass distribution shown in the spectrum of Fig. 2.16, revealing the presence of C_{10} to C_{30} species, is in good agreement with those observed in previous studies of graphite-ablated plasma at similar excitation conditions [116]. The restriction of cluster sizes to small-sized carbon nanoparticles has also been reported in [117], where it was argued that stronger excitation conditions are necessary to observe clusters larger than C_{32}. In that case, one should expect the appearance of closed cages made of joined five and six member rings. It was confirmed that C_{60} and C_{70} fullerenes, are the most abundant species among the high-mass ions of the carbon plasma plumes at higher ablation fluences. It was also suggested [116] that it is very likely that the plasma is sufficiently dense for cluster growth to occur via ion-molecular reactions. The kinetic mechanism can be responsible for the formation of carbon cluster ions since the supersonic entrainment method is expected to considerably cool down the cluster ions. The growth of clusters is based on the addition of many small carbon neutral species to the ions in a stepwise fashion.

An explanation for strong harmonic generation from nanoparticles compared with single atoms or ions could be the higher concentration of neutral atoms inevitably accompanying the presence of nanoparticles. Unlike single atoms and ions, whose density quickly decreases due to plasma expansion, nanoparticles retain local densities that are close to solid state. The increase of electron recombination cross-section for clusters with respect to atoms can also potentially enhance the HHG efficiency in nanoparticle-contained plasmas. Earlier studies of HHG from gases [101, 118, 119], as well as from plasmas containing various nanoparticles (Ag, Au, $BaTiO_3$, etc) [67, 69], have proven these assumptions by demonstrating the enhanced HHG from clusters as compared with single atoms and ions. Further evidence of the cluster contribution to the enhancement of the harmonic generation process comes from investigations of very intense laser ablation of a silver target [48], which gave clues regarding the participation of in-situ generated nanoparticles.

The observation of a strong extended harmonic plateau in the case of the 1300 nm probe radiation also suggests the involvement of clusters in the HHG process with MIR pulses. Assuming the expected decrease of harmonic intensity from single particle emitters with the growth of driving radiation wavelength ($I_h \propto \lambda^{-5}$, [5, 102, 103, 120]), one can anticipate at least one order of magnitude decrease of harmonic yield from MIR pulses as compared with the yield obtained with 780 nm radiation at other equal conditions, in particular, pulse energy and duration. However, the experiment did not show a considerable difference between the intensities of harmonics originated from these two driving sources (Fig. 2.13). The energy of the 1300 nm pulses in the plasma area (0.2 mJ) was lower than the Ti:sapphire pulse

(0.54 mJ). This suggests the involvement of a mechanism, which compensates for the expected considerable decrease of harmonic efficiency for the longer-wavelength laser. The involvement of a clustered component of the laser plasma in the process of frequency up-conversion may arguably explain the observed inconsistence with the theoretical predictions of the $I_h \propto \lambda^{-5}$ rule defined for atomic species [102, 103].

In principle, the intensity enhancement of the harmonic spectrum from the carbon plume in the 15–26 eV range invokes the involvement of surface plasmon resonances of nanoparticles, analogously to the case of fullerenes [51, 69] in the range of their giant resonance in the vicinity of 20 eV. To prove this in the case of carbon plasma, one should provide evidence of giant absorption in the above range, but this has not been reported yet in the literature. The plasmonic properties of carbon nanoparticles can be responsible for the observed enhancement of carbon harmonics, however their role requires additional study [121]. Another option for explaining the high harmonic generation yield in the carbon plume is the indirect involvement of the clusters in HHG that, while not participating as harmonic emitters, could rather enhance the local field, analogously to recently reported studies using gold nanostructures enhancing gas HHG [122, 123].

As it was mentioned, recent comparative studies of lower-order harmonic efficiency in argon gas and carbon plasmas have revealed stronger conversion efficiency in the carbon plasmas [66]. In this section, we have discussed evidence of the superior properties of graphite ablation for HHG. Some arguments which could explain the enhanced high harmonic yield from this medium are as follows: (a) the graphite target allows easier generation of a relatively dense carbon plasma and the production of adequate phase-matching conditions for lower-order harmonic generation, (b) the first ionization potential of carbon is high enough to prevent the appearance of high concentration of free electrons, a condition that is not necessarily met in metal plasma plumes, (c) neutral carbon atoms dominate in the carbon plume at optimal conditions of HHG before the interaction with the femtosecond laser pulse, and (d) carbon species allow the formation of multi-particle clusters during laser ablation, which can enhance the HHG yield.

2.5 Harmonic Generation in Fullerenes Using Few- and Multi-Cycle Pulses of Different Wavelengths

Fullerenes can be considered as an attractive nonlinear medium for the HHG. Their relatively large sizes and broadband surface plasmon resonance (SPR) in the XUV range allowed the first demonstration of enhanced HHG near the SPR of C_{60} ($\lambda_{SPR} \approx$ 60 nm, with 10 nm full width at half maximum) [32]. The application of laser ablation technique allowed the creation of C_{60}-rich plasma ($\sim 5 \times 10^{16}\,\mathrm{cm}^{-3}$), in a stark contrast with the density $<10^{14}\,\mathrm{cm}^{-3}$ which can be achieved using the heat oven based methods of production of the fullerene beams.

The theoretical studies of HHG from C_{60} using the multi-cycle pulses include the extension of three-step model [124], analysis of the electron constrained over

the surface of a rigid sphere, with geometrical parameters similar to those of the C_{60} [125], and application of dynamical simulations [126]. In the latter work, high-order harmonics were shown to be due to multiple excitations and could be easily generated even with a weak laser field. Those studies reveal how HHG can be used to probe the electronic and molecular structure of C_{60}. At the same time, theoretical investigation of such systems is hampered by the fact that the Hamiltonian of HHG is time dependent and the system consists of many electrons. The investigation of the influence of the electrons on the resonant HHG can be performed by means of a multiconfigurational time-dependent Hartree-Fock (MCTDHF) approach, which has the accuracy of direct numerical solution of Schrödinger equation and is almost as simple as the ordinary time-dependent Hartree-Fock approach. In particular, the computations could be based on the multiconfigurational time-dependent Hartree software packages. In [46], simulations of resonant HHG were performed by means of a MCTDHF approach for three-dimensional fullerene-like systems. The influence of the SPR of C_{60} on the harmonic efficiency in the range of 60 nm ($E = 20$ eV) was analysed and showed the ways of resonant HHG optimisation [127].

The saturation intensities of different charge states of C_{60} are higher compared to isolated atoms of similar ionisation potential. In this connection, it would be interesting to analyse the behaviour of fullerene molecules in the field of few-cycle pulses from the point of view of harmonic generation and compare these studies with those carried out using the multi-cycle pulses. The motivation of studies [128] was to analyse the conditions of efficient HHG from the plasma containing C_{60}, when picosecond radiation ablates the fullerene-containing target at high pulse repetition rate (1 kHz) and then few-cycle pulse ($t = 3.5$ fs) propagates through the fullerene plasma. It would be also interesting to analyse HHG in fullerenes using the longer- and shorter-wavelengths probe sources, in particular using the 1300 and 780 nm multi-cycle (35 and 40 fs) pulses.

The detailed description of experimental setup for plasma HHG is presented in previous sections. Briefly, a small part ($E = 120\,\mu$J) of the uncompressed radiation of a 1 kHz Ti:sapphire laser with central wavelength 780 nm and pulse duration 8 ps was split from the beam line prior to the laser compressor stage and was focused into the vacuum chamber to create a plasma on the C_{60}-containing target using an intensity on the target surface of typically $I_{ps} = 2 \times 10^{10}$ W cm^{-2}. Then the few-cycle pulses were focused into the plasma plume, approximately $150 - 200\,\mu$m above the target surface, to generate high-order harmonics. Two types of targets (C_{60} powder glued on the glass substrates or rotating aluminium rod, and bulk graphite) were used for plasma harmonics generation. These targets were studied from the point of view of comparative intensities of harmonics they can provide. The harmonic spectra from the plasmas produced on the bulk graphite and fullerene powder glued onto the glass surface are presented in Fig. 2.17. The harmonics up to the 29th order were obtained from the fullerene plasma. Note that harmonic efficiency in the case of graphite plasma was a few times stronger compared with the case of fullerene plasma, which probably was caused by higher concentration of plasma in the former case, as it has also been reported in [62].

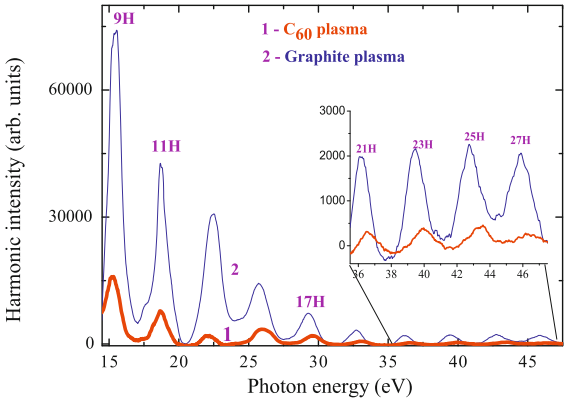

Fig. 2.17 Harmonic spectra from fullerene (*thick curve*) and graphite (*thin curve*) plasmas using the heating 8 ps pulses at identical experimental conditions. Reproduced from [128] with permission from Optical Society of America

The results of comparative studies of the HHG in fullerene plasma using the few-cycle (3.5 fs) and multi-cycle (40 fs) pulses are presented in Fig. 2.18. In the latter case, the Ti:sapphire laser generating the 1 kHz, 4 mJ, 40 fs pulses was used. The conversion efficiency of the 40 fs pulses at the beginning of plateau range in the case of plasma plume containing fullerenes was estimated to be $\sim 5 \times 10^{-6}$ using the comparison with the HHG conversion efficiency in the silver plasma, which has previously been reported at analogous experimental conditions to be 1×10^{-5} [36]. One can see that the cut-off in the case of longer pulses (25th harmonic) was shorter with regard to the few-cycle pulses (29th harmonic).

The problem of using fullerene powder-containing target is a shot-to-shot instability and rapid decrease of harmonic yield, due to abrupt change in the target morphology. This negative feature of harmonics from such targets prevents from using these intense harmonic sources in applications. Nevertheless, currently HHG in laser-produced plasma plumes remains the alone method of studies of the high-order nonlinearities of fullerenes. The alternative could be a creation of long homogeneous

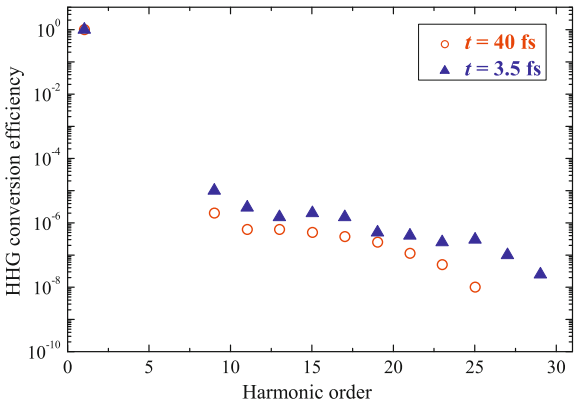

Fig. 2.18 Comparison of HHG conversion efficiencies from fullerene plasma using the 3.5 fs (*triangles*) and 40 fs (*circles*) pulses. Reproduced from [128] with permission from Optical Society of America

tapes containing fullerenes, which continuously move from shot to shot to provide the fresh surface for each next laser pulse. The application of rotating targets containing C_{60} is another method for improvement of the harmonic stability from this medium, which was implemented in these studies. The application of rotating aluminium rods as the substrates on which the fullerene powder was glued considerably improved a stability of harmonics from C_{60}-containing plasmas compared with the case of ablated layer of fullerene powder glued on the fixed glass substrate. One can note that, once the rotating rod stops, the harmonic efficiency from fullerene plasma decreased to almost zero level during 1–2 s. The proposed technique, which was described in the case of bulk targets in previous sections, could be very useful in the case of powder-like targets (fullerenes, metal nanoparticles, organic powder-like samples, etc).

As it was mentioned, the conversion efficiency studies showed advantages of HHG in the case of graphite plasma compared with fullerene plasma [62]. This advantage of graphite plasma over fullerene one can be explained by different concentrations of particles in these plasmas. The concentration of fullerenes can be considered as below $10^{17}\,\mathrm{cm}^{-3}$ [32], while the estimates of carbon plasma based on a three-dimensional molecular dynamical simulation of laser ablation of graphite using the molecular dynamics code ITAP IMD [112] showed that, in the case of heating by 8 ps pulses, the graphite plasma density can reach $2.6 \times 10^{17}\,\mathrm{cm}^{-3}$ at the moderate intensity ($2 \times 10^{10}\,\mathrm{W\,cm}^{-2}$) of heating radiation [66]. This difference in plasma densities can be instrumental in explanation of the observed higher efficiency of HHG from graphite plasma compared with fullerene one. Another reason for observed advanced features of graphite plasma harmonics could be the cluster formation during laser ablation (see previous section).

In order to analyse the harmonic yield of the mid infrared source in the fullerene-contained plasma an optical parametric oscillator pumped by the 40 fs Ti:sapphire laser was used. Figure 2.19 shows the comparison of fullerene harmonic spectra generated in the case of 1300 and 780 nm multi-cycle probe pulses. Harmonics up to the 41st order (Fig. 2.19, bottom panel) were observed in the case of 1300 nm probe pulses at the conditions of optimal plasma formation using the heating 160 ps pulses. Over-excitation of target by 160 ps pulses (Fig. 2.19, middle panel) led to appearance of plasma emission in the 25–45 eV range of photon energies ($\lambda = 27 - 50$ nm). At these conditions, no harmonics were observed during propagation of femtosecond pulses through such over-excited plasma.

Harmonic spectrum up to the 25th order in the case of 780 nm, 40 fs probe pulses is presented in the Fig. 2.19 (upper panel). One can clearly see the extension of harmonic cut-off in the case of longer-wavelength probe pulses by comparing the harmonic spectra generated using the 780 and 1300 nm probe pulses. The plasma harmonic yields from the 780 and MIR probe pulses followed approximately the expected $I_h \propto \lambda^{-5}$ rule. The harmonic efficiency of the XUV radiation driven by MIR pulses was 7–15 times less compared with the case of 780 nm probe pulses, which is comparable with the expected ratio between harmonic intensities from these sources [$(1300/780)^5 \approx 12.7$] followed from above rule, assuming approximately equal energies of the 780 and 1300 nm pulses (0.53 and 0.5 mJ respectively).

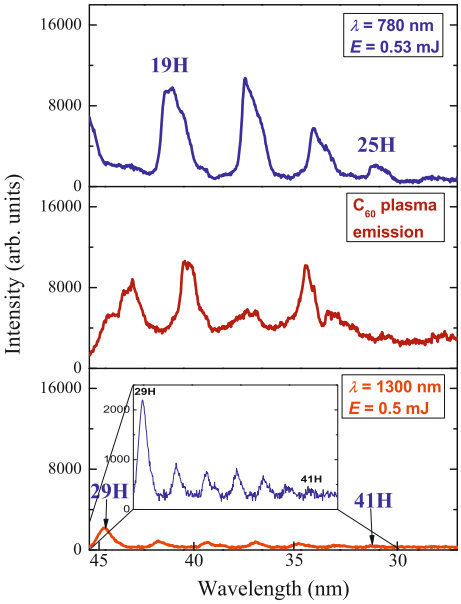

Fig. 2.19 Comparative harmonic spectra from fullerene-contained plume using the 780 nm (*upper panel*) and 1300 nm (*bottom panel*) multi-cycle pulses. Note the equal Y axes for these cases. The middle panel shows C_{60} plasma emission spectrum at over-excitation of target by 160 ps pulses, without further excitation by femtosecond probe pulses. Reproduced from [128] with permission from Optical Society of America

Previous HHG studies in fullerenes were performed using the multi-cycle pulses (30 fs [32], 48 fs [129], and 110 fs [60]). The stability of C_{60} against fragmentation in these multi-cycle laser fields led to fast diffusion of the excitation energy. Even better conditions can occur in the case of few-cycle pulses used for fullerene HHG. In that case fullerenes can withstand the influence of the strong field of few-cycle pulses due to the growth of saturation intensity. This can further increase the diffusion of the excitation energy within the fullerenes due to their very large number of internal degrees of freedom. The increase of energy diffusion should follow with the decrease of disintegration of fullerenes, which enhances the probability of harmonic emission from these clusters.

The carbon, which was compared in these experiments with C_{60}, can easily be aggregated during laser ablation, thus providing the nanoparticles in laser plume (see previous section). In that case the comparison of two clustered species (large 5–20 nm carbon clusters and 0.7 nm C_{60}) can lead to their different nonlinear optical response once the interacting laser pulse becomes compressed from the multi-cycle to few-cycle duration. Above-presented results show that application of shortest pulses changes the dynamics of fullerene behaviour leading to increase of the HHG cut-off, while the intensity of 'fullerene harmonics' became less compared with 'carbon harmonics'. As we mentioned, the additional reason of this could be different concentrations of harmonic emitters from two plasma plumes. It was difficult to maintain equal plasma concentrations in these two cases, since no reliable methods are existed, which could define the exact concentrations of carbon and fullerene plasmas at different 'optimal' conditions of HHG from these media.

The intensity of probe femtosecond pulse is crucial for optimizing the HHG from C_{60}. Increasing the intensity of this pulse did not lead to an extension of the harmonic cutoff from the fullerene plume, which is a signature of HHG saturation in the medium. Moreover, at relatively high femtosecond laser intensities, one can observe a decrease in the harmonic output, which can be ascribed to the phase mismatch caused by propagation effects.

The stability of C_{60} molecules against ionization and fragmentation is of particular importance, especially for their application as a medium for HHG using laser pulses of different duration. Because of this the structural integrity of the fullerenes ablated off the surface should be intact until the probe pulse arrives. Hence, the heating pulse intensity also becomes a sensitive parameter. At lower intensities the concentration of the clusters in the plume would be low, while at higher intensities one can expect fragmentation. This phenomenon is observed when the heating pulse intensity on the surface of fullerene-rich targets is increased above the critical value (Fig. 2.19, middle panel). The abrupt reduction in harmonic intensity in that case can be attributed to phenomena such as fragmentation of fullerenes, increase in free electron density, and self-defocusing, both leading to the phase mismatch of HHG.

2.6 Isolated Sub-Femtosecond XUV Pulse Generation in Mn Plasma Ablation

In this section, we discuss HHG from transition metal plasmas. These are very promising targets in view of the giant resonances found in the photoionization cross sections. For example, the Mn^+ cross section is ~40 Mb at 50 eV photon energy [130], whereas rare gas atoms have cross sections between 1 and 8 Mb at this photon energy [131]. Photorecombination—the third step in the recollision model—is the inverse process of photoionization [132] and therefore HHG and photoionization must exhibit the same resonances. This has been confirmed not only by previous resonance-induced experiments with laser-produced transition metal plasmas but also in a recent study of HHG from xenon gas [133].

Resonance-induced enhancement of a single harmonic of the laser radiation allowed considerable improvement of harmonic efficiency in some specific XUV spectral ranges related with high oscillator strengths of ionic states of metals. This was confirmed in multiple studies following the initial observation of this phenomenon in indium plasma [25]. In particular, the strong enhancement of a single harmonic was reported in Cr [28], and Mn [35] plasmas. The Mn plasma is of special interest since it showed the highest harmonic cut-off energy observed in plasma plumes (101st harmonic [35]). In previous studies multi-cycle (30 [35] and 140 fs [134]) laser pulses were employed and the generation of all harmonics in the plateau was observed together with a strongly enhanced single harmonic.

Recent progress in the generation of few-cycle pulses allowed the observation of various new effects including the realisation of isolated attosecond-pulse generation

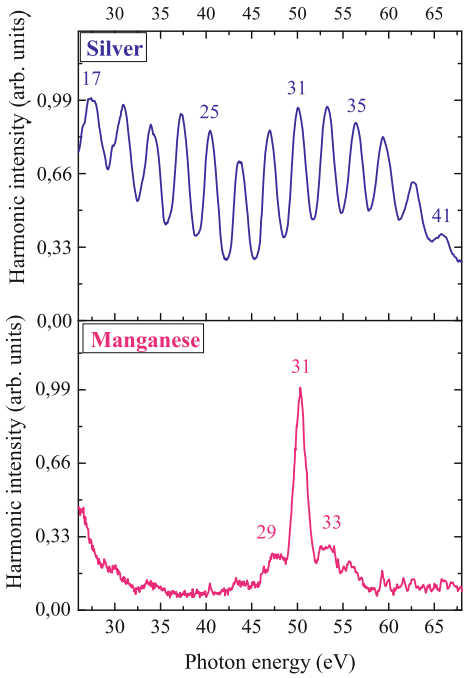

Fig. 2.20 Harmonic spectra from the silver plasma (*upper curve*) and manganese plasma (*bottom curve*). Reproduced from [138] with permission from Optical Society of America

in gas media [135–137]. In this connection it is interesting to analyse resonance-induced processes observed in an ablation plume using the shortest available drive laser pulses. Below, we present the analysis of resonance enhancement in manganese plasmas using 3.5 fs pulses [138]. The most interesting feature observed in those experiments was a suppression of almost all neighbouring harmonics in the vicinity of a resonantly enhanced single harmonic at the photon energy of ~50 eV.

The experimental arrangements were analogous to those presented in Sects. 2.3 and 2.4 of this chapter. The harmonic spectrum in the case of propagation of 3.5 fs pulses through the manganese plasma was strikingly different compared with other plasma samples (for example Ag plasma) analysed in separate experiments. While all other samples studied showed the relatively featureless harmonic spectra with extended cut-offs (Fig. 2.20, upper curve showing the spectrum of harmonics generating in the silver plasma), the Mn plasma allowed the generation of a strong single harmonic substantially enhanced compared with neighbouring ones (Fig. 2.20, bottom curve).

One can note that in earlier work the harmonic spectra from manganese plasmas for 30 fs [35] and 140 fs [134] pulses also showed enhanced harmonics around 50 eV. The assumption of the resonance nature of the enhancement of harmonics of the ~800 nm radiation of Ti:sapphire lasers in this spectral region is supported by the presence of a strong giant resonance in the vicinity of 50 eV confirmed by experimental [130, 139] and theoretical [140] studies. The enhancement of a single harmonic

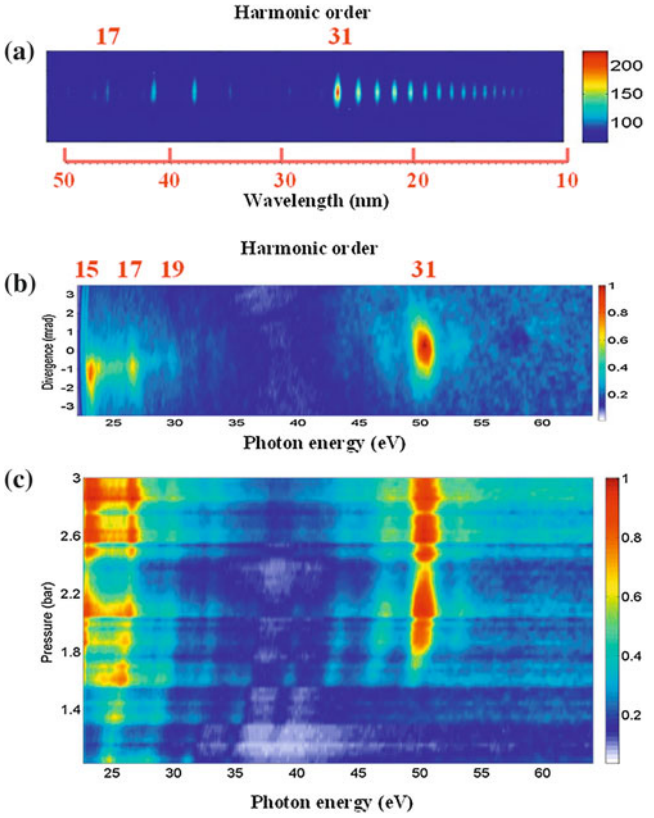

Fig. 2.21 Raw images of harmonic spectra from manganese plasma in the case of (**a**) 40 fs and (**b**) 3.5 fs probe pulses obtained at the same intensity. (**c**) Raw images of harmonic spectra from Mn plasma at different pressures of neon in the hollow fiber obtained at the same energy of probe laser pulses. Reproduced from [138] with permission from Optical Society of America

can be attributed to the broadband resonances of the ions of few metals, such as V, In, Cd, Cr, Cd, and Mn. These "giant" resonances have been experimentally confirmed in the literature [130, 139, 141] and discussed recently in a few theoretical studies [46, 90–93].

However, in previous studies using multi-cycle drive pulses, the intensity of enhanced harmonics was only a few times higher than neighboring harmonic orders. The same features were reproduced in the reviewed studies using 40 fs pulses from another Ti:sapphire laser at similar intensity inside the laser plasma (4×10^{14} W cm^{-2}). The raw image of the harmonic spectrum presented in Fig. 2.21a shows several enhanced harmonics starting from the 31st order followed by an extended second plateau. The extension of the harmonic cutoff exceeding the 71st order is attributed to the involvement of doubly charged Mn ions as the sources of HHG. This feature of Mn plasma harmonics has already been reported earlier [35].

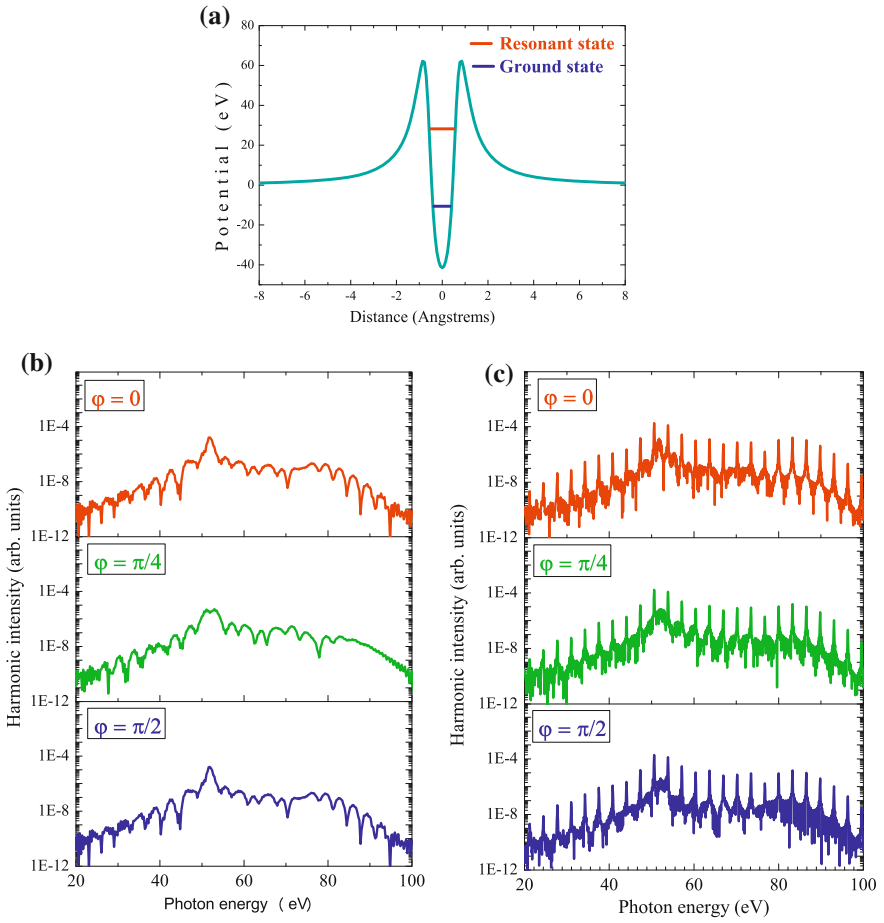

Fig. 2.22 **a** Potential used for the numerical simulations. **b**, **c** Calculated HHG spectra using **b** a long (40 fs) pulse and **c** few-cycle pulses at different values of the CEP ($\phi = 0$, $\pi/4$, and $\pi/2$). Reproduced from [138] with permission from Optical Society of America

Here also presented a typical image of a Mn harmonic spectrum in the case of 3.5 fs pulses (Fig. 2.21b). No second plateau, which was seen in the case of multi-cycle (40 fs) pulses, is observed for the few-cycle pulse. Most striking was the observation of a single, very strong, broadband (2.5 eV) 31st harmonic. Only two weak neighboring harmonics (around the strong emission) are seen in the 30–65 eV spectral range. The ratio between the intensities of the enhanced harmonic to the weak neighboring harmonics exceeded one order of magnitude. One can note that, at a lower intensity of the femtosecond pulse ($<2 \times 10^{14}$ W cm^{-2}), this strong harmonic disappeared when using both multi- and few-cycle pulses.

The distinctive structure of the harmonic spectra, both for 40 and 3.5 fs pulses, clearly points to the involvement of Mn resonances centred around 50–51 eV. The

same can be said about the photoionization or photoabsorption characteristics of Mn^+ plasma, which are due to the 'giant' $3p \rightarrow 3d$ resonance [130]. The laser polarization dependence of this emission was analyzed and it was found that the 50 eV radiation abruptly disappears with the change of the polarization state of the femtosecond probe pulses from linear to circular, which is a clear signature of the emission being due to high harmonic generation.

To analyse the effect of the spectro-temporal characteristics of the femtosecond radiation on the harmonic yield, the pressure of neon in the hollow fiber of second compressor was varied, thus changing the duration of the harmonic drive pulse [106]. The spectral and intensity variations of manganese harmonic spectra in the range of 22–62 eV as the functions of neon pressure in the hollow fiber are shown in Fig. 2.21c. One can clearly see that, with change of pressure (from 1 to 2.3 bar), the single 31st harmonic intensity varies from almost zero to its maximum high value. A blue shift of the harmonics is also evident. Further increase of neon pressure up to 3 bar, at which the experiments with the 3.5 fs pulses were carried out, did not change the harmonic distribution.

In the following, the results of numerical simulations within a one-dimensional model are presented. It was assumed that the main contribution to the resonant peak in the spectrum comes from Mn^+ ions. Note that the ionisation potential of Mn^{2+} ions (33.7 eV) is more than twice higher than the ionisation potential of Mn^+ ions (15.6 eV). The time-dependent Schrödinger equation was solved by means of the split-operator method [90, 93, 142]. The metastable state of this model potential is at 51.8 eV above the ground state (Fig. 2.22a). The laser field is $E(t) = E_0 f(t) \cos(\omega_0 t + \varphi)$, where $f(t)$ is the pulse envelope, φ denotes the carrier envelope phase (CEP) and ω_0 is the laser frequency corresponding to the central wavelength $\lambda = 770$ nm. The laser intensity is $I_0 = 4 \times 10^{14}$ W cm^{-2}. A CEP of $\varphi = 0$ means that the maximum of the envelope corresponds to a maximum of sin $(\omega_0 t)$.

HHG spectra were calculated for pulse shapes with different lengths and for different values of φ (Fig. 2.22b,c). A $\sin^2$ envelope with a total length of 4 full cycles was used to model the 3.5 fs pulse, while an envelope with 13 cycles of constant intensity and 21 cycles of total duration was used to model the 40 fs case. The long pulse led to a HHG spectrum that shows well defined peaks at the odd harmonic orders and that is weakly dependent on the CEP (Fig. 2.22b). Figure 2.22c shows the dependence of the harmonic spectrum on the CEP in the case of the short, few-cycle pulse. In all cases, the resonance dominated the HHG spectrum. The most intense emission was occurred around 51 eV, where the metastable state is located. Although some difference between harmonic spectra for $\varphi = 0$, $\pi/4$, and $\pi/2$ is found, one can note that the CEP dependence is strongest for the spectrum outside the region of the resonance. For random CEP the substructure of the spectrum will average out as confirmed by numerical averaging over 20 values of the CEP in the range from 0 to π. The resonance peak itself depends less on the CEP.

The experiments described above were carried out without CEP stabilisation (that is, for random CEP values). The HHG experiments with Mn plasma using 3.5 fs pulses were also performed with stabilized CEP ($\varphi = 0$ and $\pi/2$) and no specific differences

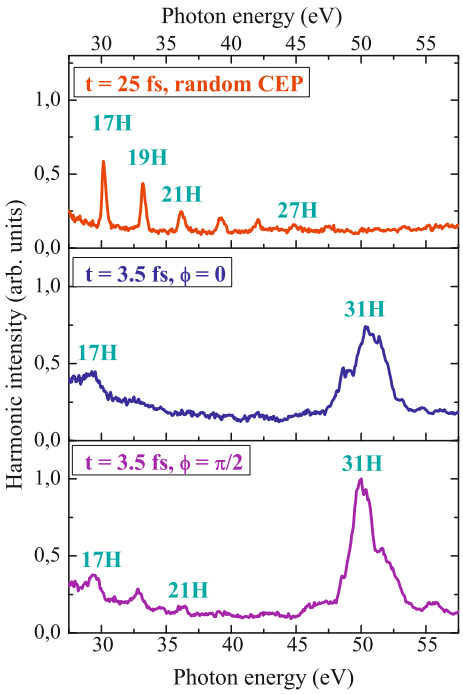

Fig. 2.23 Experimental harmonic spectra generated from manganese plasma in the case of the absence of gas in the hollow fibre compressor ($t = 25$ fs) and random CEP (*upper panel*), and at 3 bar pressure ($t = 3.5$ fs) at fixed CEP ($\varphi = 0$, *middle panel*; $\varphi = \pi/2$, *bottom panel*). Reproduced from [138] with permission from Optical Society of America

were found in that case (Fig. 2.23), though some variation of harmonic distribution was observed for the lower order harmonics (compare the middle and bottom curves of Fig. 2.23). The spectral shapes of the 31st harmonic emission were similar for these two fixed values of CEP, while a considerable difference in harmonic spectra was maintained when comparing to longer pulse duration and lower intensity of the driving pulses. Figure 2.23 shows HHG measurements for 25 fs pulses (upper panel) and 3.5 fs pulses (middle and bottom panels) of the same energy. One can clearly see the absence of harmonic extension and resonance-induced HHG in the case of low-intensity, 25 fs pulses.

The fact that a strong CEP dependence of the harmonic spectra in the case of 3.5 fs pulses was not observed could also be attributed to the presence of a significant density of free electrons in the manganese plasma, which might diminish the difference between the HHG spectra recorded for different values of experimental CEP. The same can be said about other HHG experiments using silver and brass plasmas, which did not show significant differences in harmonic spectra when comparing few-cycle pulses with fixed and random CEP. Comparative studies with gas media under similar experimental conditions were carried out and found a characteristic dependence of the HHG spectra on the CEP. Thus the absence of the strong influence of the CEP on the harmonic pattern generated by few-cycle pulses from the ablation plumes appears to be a common feature of plasma HHG.

References

1. G.D. Tsakiris, K.K. Eidmann, J. Meyer-ter-Vehn, F. Krausz, New J. Phys. **8**, 19 (2006)
2. B. Dromey, M. Zepf, A. Gopal, K. Lancaster, M.S. Wei, K. Krushelnick, M. Tatarakis, N. Vakakis, S. Moustaizis, R. Kodama, M. Tampo, C. Stoeckl, R. Clarke, H. Habara, D. Neely, S. Karsch, P. Norreys, Nature Phys. **2**, 456 (2006)
3. D.H. Reitze, S. Kazamias, F. Weihe, G. Mullot, D. Douillet, F. Aug, O. Albert, V. Ramanathan, J.P. Chambaret, D. Hulin, P. Balcou, Opt. Lett. **29**, 86 (2004)
4. T. Pfeifer, D. Walter, C. Winterfeldt, C. Spielmann, G. Gerber, Appl. Phys. B **80**, 277 (2005)
5. C.A. Froud, E.T.F. Rogers, D.C. Hanna, W.S. Brocklesby, M. Praeger, A.M. de Paula, J.J. Baumberg, Opt. Lett. **31**, 374 (2006)
6. E.A. Gibson, A. Paul, N. Wagner, R. Tobey, D. Gaudiosi, S. Backus, I.P. Christov, A. Aquila, E.M. Gullikson, D.T. Attwood, M.M. Murnane, H.C. Kapteyn, Science **302**, 95 (2003)
7. S. Kazamias, D. Douillet, F. Weihe, C. Valentin, A. Rousse, S. Sebban, G. Grillon, F. Auge, D. Hulin, P. Balcou, Phys. Rev. Lett. **90**, 193901 (2003)
8. U. Teubner, G. Pretzler, T. Schlegel, K. Eidmann, E. Förster, K. Witte, Phys. Rev. A **67**, 013816 (2003)
9. P.A. Norreys, M. Zepf, S. Moustaizis, A.P. Fews, J. Zhang, P. Lee, M. Bakarezos, C.N. Danson, A. Dyson, P. Gibbon, P. Loukakos, D. Neely, F.N. Walsh, J.S. Wark, A.E. Dangor, Phys. Rev. Lett. **76**, 1832 (1996)
10. G.J. Pert, Phys. Rev. A **75**, 023808 (2007)
11. T. Ozaki, R.A. Ganeev, A. Ishizawa, T. Kanai, H. Kuroda, Phys. Rev. Lett. **89**, 253902 (2002)
12. F. Gruner, S. Becker, U. Schramm, T. Eichner, M. Fuchs, R. Weingartner, D. Habs, J. Meyer-ter-Vehn, M. Geissler, M. Ferrario, Appl. Phys. B **86**, 431 (2007)
13. P.B. Corkum, F. Krausz, Nature Phys. **3**, 381 (2007)
14. C. Figueira de Morisson Faria, R. Kopold, W. Becker, J.M. Rost, Phys. Rev. A **65**, 023404 (2002)
15. R. Taieb, V. Véniard, J. Wassaf, A. Maquet, Phys. Rev. A **68**, 033403 (2003)
16. V.P. Silin, P.V. Silin, Phys. Uspekhi **50**, 729 (2007)
17. Y. Akiyama, K. Midorikawa, Y. Matsunawa, Y. Nagata, M. Obara, H. Tashiro, K. Toyoda, Phys. Rev. Lett. **69**, 2176 (1992)
18. S. Kubodera, Y. Nagata, Y. Akiyama, K. Midorikawa, M. Obara, H. Tashiro, K. Toyoda, Phys. Rev. A **48**, 4576 (1993)
19. C.-G. Wahlströom, S. Borgström, J. Larsson, S.-G. Pettersson, Phys. Rev. A **51**, 585 (1995)
20. W. Theobald, C. Wülker, F.R. Schäfer, B.N. Chichkov, Opt. Commun. **120**, 177 (1995)
21. R.A. Ganeev, V.I. Redkorechev, T. Usmanov, Opt. Commun. **135**, 251 (1997)
22. K. Krushelnick, W. Tighe, S. Suckewer, JOSA B **14**, 1687 (1997)
23. P.B. Corkum, Phys. Rev. Lett. **71**, 1994 (1993)
24. R.A. Ganeev, M. Suzuki, M. Baba, H. Kuroda, T. Ozaki, Opt. Lett. **30**, 768 (2005)
25. R.A. Ganeev, M. Suzuki, T. Ozaki, M. Baba, H. Kuroda, Opt. Lett. **31**, 1699 (2006)
26. R.A. Ganeev, H. Singhal, P.A. Naik, V. Arora, U. Chakravarty, J.A. Chakera, R.A. Khan, I.A. Kulagin, P.V. Redkin, M. Raghuramaiah, P.D. Gupta, Phys. Rev. A **74**, 063824 (2006)
27. R.A. Ganeev, M. Baba, M. Suzuki, H. Kuroda, J. Appl. Phys. **99**, 103303 (2006)
28. R.A. Ganeev, P.A. Naik, H. Singhal, J.A. Chakera, P.D. Gupta, Opt. Lett. **32**, 65 (2007)
29. R.A. Ganeev, M. Suzuki, M. Baba, H. Kuroda, Appl. Phys. B **81**, 1081 (2005)
30. R.A. Ganeev, H. Singhal, P.A. Naik, V. Arora, U. Chakravarty, J.A. Chakera, R.A. Khan, P.V. Redkin, M. Raghuramaiah, P.D. Gupta, J. Opt. Soc. Am. B **23**, 2535 (2006)
31. M. Suzuki, M. Baba, R. Ganeev, H. Kuroda, T. Ozaki, Opt. Lett. **31**, 3306 (2006)
32. R.A. Ganeev, L.B. Elouga Bom, J. Abdul-Hadi, M.C.H. Wong, J.P. Brichta, V.R. Bhardwaj, T. Ozaki, Phys. Rev. Lett. **102**, 013903 (2009)
33. R.A. Ganeev, H. Singhal, P.A. Naik, U. Chakravarty, V. Arora, J.A. Chakera, R.A. Khan, M. Raghuramaiah, S.R. Kumbhare, R.P. Kushwaha, P.D. Gupta, Appl. Phys. B **87**, 243 (2007)
34. M. Suzuki, M. Baba, H. Kuroda, R.A. Ganeev, L.B. Elouga Bom, T. Ozaki, Opt. Express **15**, 4112 (2007)

35. R.A. Ganeev, L.B. Elouga Bom, J.-C. Kieffer, T. Ozaki, Phys. Rev. A **76**, 023831 (2007)
36. R.A. Ganeev, M. Baba, M. Suzuki, H. Kuroda, Phys. Lett. A **339**, 103 (2005)
37. L.B. Elouga Bom, J.-C. Kieffer, R.A. Ganeev, M. Suzuki, H. Kuroda, T. Ozaki, Phys. Rev. A **75**, 033804 (2007)
38. R.A. Ganeev, L.B. Elouga Bom, J.-C. Kieffer, T. Ozaki, Phys. Rev. A **75**, 063806 (2007)
39. R.A. Ganeev, M. Suzuki, M. Baba, H. Kuroda, Phys. Rev. A **76**, 023805 (2007)
40. R.A. Ganeev, M. Suzuki, P.V. Redkin, M. Baba, H. Kuroda, Phys. Rev. A **76**, 023832 (2007)
41. R.A. Ganeev, Laser Phys. **18**, 1009 (2008)
42. R.A. Ganeev, Phys. Uspekhi **52**, 55 (2009)
43. R.A. Ganeev, H. Singhal, P.A. Naik, I.A. Kulagin, P.V. Redkin, J.A. Chakera, M. Tayyab, R.A. Khan, P.D. Gupta, Phys. Rev. A **80**, 033845 (2009)
44. R.A. Ganeev, H. Singhal, P.A. Naik, J.A. Chakera, M. Tayyab, M. Baba, H. Kuroda, P.D. Gupta, J. Opt. Soc. Am. B **26**, 2143 (2009)
45. R.A. Ganeev, M. Baba, T. Ozaki, H. Kuroda, J. Opt. Soc. Am. B **27**, 1077 (2010)
46. P.V. Redkin, R.A. Ganeev, Phys. Rev. A **81**, 063825 (2010)
47. R.A. Ganeev, H. Singhal, P.A. Naik, J.A. Chakera, A.K. Srivastava, T.S. Dhami, M.P. Joshi, P.D. Gupta, Appl. Phys. B **100**, 581 (2010)
48. H. Singhal, R.A. Ganeev, P.A. Naik, J.A. Chakera, U. Chakravarty, H.S. Vora, A.K. Srivastava, C. Mukherjee, C.P. Navathe, S.K. Deb, P.D. Gupta, Phys. Rev. A **82**, 043821 (2010)
49. R.A. Ganeev, H. Singhal, P.A. Naik, J.A. Chakera, H.S. Vora, R.A. Khan, P.D. Gupta, Phys. Rev. A **82**, 053831 (2010)
50. P.V. Redkin, M.K. Kodirov, R.A. Ganeev, JOSA B **18**, 165 (2011)
51. R.A. Ganeev, Laser Phys. **21**, 25 (2011)
52. R.A. Ganeev, P.A. Naik, H. Singhal, J.A. Chakera, M. Kumar, M.P. Joshi, A.K. Srivastava, P.D. Gupta, Phys. Rev. A **83**, 013820 (2011)
53. R.A. Ganeev, P.A. Naik, J.A. Chakera, H. Singhal, N.C. Pramanik, P.A. Abraham, N. Rani Panicker, M. Kumar, P.D. Gupta, J. Opt. Soc. Am. B **28**, 360 (2011)
54. R.A. Ganeev, Opt. Spectrosc. **110**, 637 (2011)
55. R.A. Ganeev, H. Kuroda, Appl. Phys. B **103**, 151 (2011)
56. R.A. Ganeev, C. Hutchison, T. Siegel, M.E. López-Arias, A. Zaïr, J.P. Marangos, J. Modern Opt. **58**, 819 (2011)
57. R.A. Ganeev, C. Hutchison, T. Siegel, A. Zaïr, J.P. Marangos, Phys. Rev. A **83**, 063837 (2011)
58. P.V. Redkin, M. Danailov, R.A. Ganeev, Phys. Rev. A **84**, 013407 (2011)
59. R.A. Ganeev, L.B. Elouga Bom, T. Ozaki, Phys. Plasmas **18**, 083101 (2011)
60. R.A. Ganeev, M. Baba, H. Kuroda, G.S. Boltaev, R.I. Tugushev, T. Usmanov, Eur. Phys. J. D **64**, 109 (2011)
61. L.B. Elouga Bom, Y. Pertot, V.R. Bhardwaj, T. Ozaki, Opt. Express **19**, 3077 (2011)
62. Y. Pertot, L.B. Elouga Bom, V.R. Bhardwaj, T. Ozaki, Appl. Phys. Lett. **98**, 101104 (2011)
63. Y. Pertot, S. Chen, S.D. Khan, L.B. Elouga Bom, T. Ozaki, Z. Chang, J. Phys. B: At. Mol. Opt. Phys. **45**, 074017 (2012)
64. S. Haessler, L.B. Elouga Bom, O. Gobert, J.-F. Hergott, F. Lepetit, M. Perdrix, B. Carré, T. Ozaki, P. Salières, J. Phys. B: At. Mol. Opt. Phys. **45**, 074012 (2012)
65. R.A. Ganeev, C. Hutchison, A. Zaïr, T. Witting, F. Frank, W.A. Okell, J.W.G. Tisch, J.P. Marangos, Opt. Express **20**, 90 (2012)
66. R.A. Ganeev, T. Witting, C. Hutchison, F. Frank, P.V. Redkin, W.A. Okell, D.Y. Lei, T. Roschuk, S.A. Maier, J.P. Marangos, J.W.G. Tisch, Phys. Rev. A **85**, 015807 (2012)
67. R.A. Ganeev, J. Modern Opt. **59**, 409 (2012)
68. M. López-Arias, M. Oujja, M. Sanz, R.A. Ganeev, G.S. Boltaev, N.K. Satlikov, R.I. Tugushev, T. Usmanov, M. Castillejo, J. Appl. Phys. **111**, 043111 (2012)
69. R.A. Ganeev, Laser Phys. Lett. **9**, 175 (2012)
70. R.A. Ganeev, V.V. Strelkov, C. Hutchison, A. Zaïr, D. Kilbane, M.A. Khokhlova, J.P. Marangos, Phys. Rev. A **85**, 023832 (2012)
71. M. Suzuki, M. Baba, R.A. Ganeev, L.B. Elouga Bom, H. Kuroda, T. Ozaki, J. Phys. B At. Mol. At. Phys. **45**, 065601 (2012)

72. R.A. Ganeev, P.A. Naik, H. Singhal, J.A. Chakera, M. Kumar, U. Chakravarty, P.D. Gupta, Opt. Commun. **285**, 2934 (2012)
73. C. Hutchison, R.A. Ganeev, T. Witting, F. Frank, W.A. Okell, J.W.G. Tisch, J.P. Marangos, Opt. Lett. **37**, 2064 (2012)
74. R.A. Ganeev, Open Spectrosc. J. **3**, 1 (2009)
75. R.A. Ganeev, J. Phys. B At. Mol. Opt. Phys. **40**, R213 (2007)
76. R.A. Ganeev, Laser Phys. **22**, 1177 (2012)
77. R.A. Ganeev, M. Baba, H. Kuroda, G.S. Boltaev, R.I. Tugushev, T. Usmanov, Eur. Phys. J. D **64**, 109 (2011)
78. R.A. Ganeev, G.S. Boltaev, N.K. Satlikov, T. Usmanov, J. Opt. **14**, 095202 (2012)
79. G. Raşeev, B. Leyh, H. Lefebvre-Brion, Z. Phys. D **2**, 319 (1986)
80. F. Keller, H. Lefebvre-Brion, Z. Phys. D **4**, 15 (1986)
81. M.Y. Amusia, J.-P. Connerade, Rep. Prog. Phys. **63**, 41 (2000)
82. J.F. Reintjes, *Nonlinear Optical Parametric Processes in Liquids and Gases* (Academic, New York, 1984)
83. M.B. Gaarde, K. Schafer, Phys. Rev. A **64**, 013820 (2001)
84. E.S. Toma, P. Antoine, A. de Bohan, H.G. Muller, J. Phys. B At. Mol. Opt. Phys. **32**, 5843 (1999)
85. Z. Zeng, R. Li, Y. Cheng, W. Yu, Z. Xu, Phys. Scr. **66**, 321 (2002)
86. R. Bartels, S. Backus, E. Zeek, L. Misoguti, G. Vdovin, I.P. Christov, M.M. Murnane, H.C. Kapteyn, Nature **406**, 164 (2000)
87. L. Plaja, L. Roso, J. Mod. Opt. **40**, 793 (1993)
88. P.A. Oleinikov, V.T. Platonenko, G. Ferrante, J. Exp. Theor. Phys. Lett. **60**, 246 (1994)
89. I.A. Kulagin, T. Usmanov, Opt. Lett. **34**, 2616 (2009)
90. V. Strelkov, Phys. Rev. Lett. **104**, 123901 (2010)
91. D.B. Milošević, Phys. Rev. A **81**, 023802 (2010)
92. M.Y. Frolov, N.L. Manakov, A.F. Starace, Phys. Rev. A **82**, 023424 (2010)
93. M. Tudorovskaya, M. Lein, Phys. Rev. A **84**, 013430 (2011)
94. J. Yao, B. Zeng, W. Chu, J. Ni, Y. Cheng, J. Mod. Opt. **59**, 245–249 (2012)
95. M. Ferray, A. L'Huillier, X.F. Li, L.A. Lompré, G. Mainfray, G. Manus, J. Phys. B At. Mol. Opt. Phys. **21**, L31 (1988)
96. L.A. Lompré, A. L'Huillier, M. Ferray, P. Monot, G. Mainfray, G. Manus, J. Opt. Soc. Am. B **7**, 754 (1999)
97. A. McPherson, G. Ginson, H. Jara, N. Johann, I.A. McIntyre, K. Boyer, C.K. Rhodes, J. Opt. Soc. Am. B **4**, 595 (1987)
98. A. Borot, A. Malvache, X. Chen, D. Douillet, G. Iaquianiello, T. Lefrou, P. Audebert, J.-P. Geindre, G. Mourou, F. Quéré, R. Lopez-Martens, Opt. Lett. **36**, 1461 (2011)
99. P.M. Paul, E.S. Toma, P. Breger, G. Mullot, F. Augé, P. Balcou, H.G. Muller, P. Agostini, Science **292**, 1689 (2001)
100. R. Torres, T. Siegel, L. Brugnera, I. Procino, J.G. Underwood, C. Altucci, R. Velotta, E. Springate, C. Froud, I.C.E. Turcu, M.Y. Ivanov, O. Smirnova, J.P. Marangos, Opt. Express **18**, 3174 (2010)
101. C. Vozzi, M. Nisoli, J.-P. Caumes, G. Sansone, S. Stagira, S. De Silvestri, M. Vecchiocattivi, D. Bassi, M. Pascolini, L. Poletto, P. Villoresi, G. Tondello, Appl. Phys. Lett. **86**, 111121 (2005)
102. J. Tate, T. Auguste, H.G. Muller, P. Salières, P. Agostini, L.F. DiMauro, Phys. Rev. Lett. **98**, 013901 (2007)
103. K. Schiessl, K.L. Ishikawa, E. Persson, J. Burgdörfer, Phys. Rev. Lett. **99**, 253903 (2007)
104. R.A. Ganeev, C. Hutchison, T. Witting, F. Frank, W.A. Okell, A. Zaïr, S. Weber, P.V. Redkin, D.Y. Lei, T. Roschuk, S.A. Maier, I. López-Quintás, M. Martín, M. Castillejo, J.W.G. Tisch, J.P. Marangos, J. Phys. B At. Mol. At. Phys. **45**, 165402 (2012)
105. T. Witting, F. Frank, C.A. Arrell, W.A. Okell, J.P. Marangos, J.W.G. Tisch, Opt. Lett. **36**, 1680 (2011)

106. J.S. Robinson, C.A. Haworth, H. Teng, R.A. Smith, J.P. Marangos, J.W.G. Tisch, Appl. Phys. B **85**, 525 (2006)
107. M. Sanz, M.E. López-Arias, E. Rebollar, R. de Nalda, M. Castillejo, J. Nanopart. Res. **13**, 6621 (2011)
108. R. Torres, M. Jadraque, M. Martin, Appl. Phys. A **80**, 1671 (2005)
109. M. Anselment, R.S. Smith, E. Daykin, L.F. Dimauro, Chem. Phys. Lett. **134**, 444 (1987)
110. E.A. Rohlfing, J. Chem. Phys. **89**, 6103 (1988)
111. S. Acquaviva, M.L. De Giorgi, Appl. Surf. Sci. **197–198**, 21 (2002)
112. J. Roth, F. Géahler, H.-R. Trebin, Int. J. Mod. Phys. C **11**, 317 (2000)
113. T.E. Glover, J. Opt. Soc. Am. B **20**, 125 (2003)
114. H.O. Jeschke, M.E. Garsia, K.H. Bennemann, Phys. Rev. Lett. **87**, 015003 (2001)
115. A.V. Kabashin, M. Meunier, J. Appl. Phys. **94**, 7941 (2003)
116. W.R. Creasy, J.T. Brenna, Chem. Phys. **126**, 453 (1988)
117. S.C. O'Brien, J.R. Heath, R.F. Curl, R.E. Smalley, J. Chem. Phys. **88**, 220 (1988)
118. T.D. Donnelly, T. Ditmire, K. Neuman, M.D. Perry, R.W. Falcone, Phys. Rev. Lett. **76**, 2472 (1996)
119. J.W.G. Tisch, T. Ditmire, D.J. Frasery, N. Hay, M.B. Mason, E. Springate, J.P. Marangos, M.H.R. Hutchinson, J. Phys. B At. Mol. Opt. Phys. **30**, L709 (1997)
120. A. Altucci, R. Bruzzese, C. de Lisio, M. Nisoli, S. Stagira, S. De Silvestri, O. Svelto, A. Boscolo, P. Ceccherini, L. Poletto, G. Tondello, P. Villoresi, Phys. Rev. A **61**, 021801R (2000)
121. R.A. Ganeev, L.B. Elouga Bom, T. Ozaki, J. Appl. Phys. **106**, 023104 (2009)
122. S. Kim, J. Jin, Y.-J. Kim, I.-Y. Park, Y. Kim, S.-W. Kim, Nature **453**, 757 (2008)
123. A. Husakou, S.-J. Im, J. Herrmann, Phys. Rev. A **83**, 043839 (2011)
124. M.F. Ciappina, A. Becker, A. Jaron-Becker, Phys. Rev. A **76**, 063406 (2007)
125. M. Ruggenthaler, S.V. Popruzhenko, D. Bauer, Phys. Rev. A **78**, 033413 (2008)
126. G.P. Zhang, Phys. Rev. Lett. **95**, 047401 (2005)
127. R.A. Ganeev, L.B. Elouga Bom, M.C.H. Wong, J.-P. Brichta, V.R. Bhardwaj, P.V. Redkin, T. Ozaki, Phys. Rev. A **80**, 043808 (2009)
128. R.A. Ganeev, C. Hutchison, T. Witting, F. Frank, S. Weber, W.A. Okell, E. Fiordilino, D. Cricchio, F. Persico, A. Zaïr, J. W. G. Tisch, J. P. Marangos, J. Opt. Soc. Am. B **30**, 7 (2013)
129. R.A. Ganeev, H. Singhal, P.A. Naik, J.A. Chakera, A.K. Srivastava, T.S. Dhami, M.P. Joshi, P.D. Gupta, J. Appl. Phys. **106**, 103103 (2009)
130. H. Kjeldsen, F. Folkmann, B. Kristensen, J.B. West, J.E. Hansen, J. Phys. B At. Mol. At. Phys. **37**, 1321 (2004)
131. G.V. Marr, J.B. West, At. Data Nucl. Data Tables **18**, 497 (1976)
132. J. Levesque, D. Zeidler, J.P. Marangos, P.B. Corkum, D.M. Villeneuve, Phys. Rev. Lett. **98**, 183903 (2007)
133. A.D. Shiner, B.E. Schmidt, C. Trallero-Herrero, H.J. Wörner, S. Patchkovskii, P.B. Corkum, J.-C. Kieffer, F. Légaré, D.M. Villeneuve, Nat. Phys. **7**, 464 (2011)
134. R.A. Ganeev, M. Suzuki, M. Baba, H. Kuroda, Appl. Phys. Lett. **94**, 051101 (2009)
135. M. Hentschel, R. Kienberger, C. Spielmann, G.A. Reider, N. Milosevic, T. Brabec, P.B. Corkum, U. Heinzmann, M. Drescher, F. Krausz, Nature **414**, 509 (2001)
136. T. Witting, F. Frank, W.A. Okell, C.A. Arrell, J.P. Marangos, J.W.G. Tisch, J. Phys. B At. Mol. Opt. Phys. **45**, 074014 (2012)
137. C. Altucci, J.W.G. Tisch, R. Velotta, J. Mod. Opt. **58**, 1585 (2011)
138. R.A. Ganeev, T. Witting, C. Hutchison, F. Frank, M. Tudorovskaya, M. Lein, W.A. Okell, A. Zaïr, J.P. Marangos, J.W.G. Tisch, Opt. Express **20**, 25239 (2012)
139. E.T. Kilbane, J.-P. Kennedy, P. van Mosnier, J. Kampen, Phys. B At. Mol. At. Phys. **38**, L1 (2005)
140. V.K. Dolmatov, J. Phys. B At. Mol. At. Phys. **29**, L687 (1996)
141. J.B. West, J.E. Hansen, B. Kristensen, F. Folkmann, H. Kjeldsen, J. Phys. B At. Mol. At. Phys. **36**, L327 (2003)
142. M.D. Feit, J.A. Fleck, A. Steiger, J. Comp. Phys. **47**, 412 (1982)

http://www.springer.com/978-94-007-6021-9

Nonlinear Optical Properties of Materials

Ganeev, R.A.

2013, XV, 244 p., Hardcover
ISBN: 978-94-007-6021-9